

Review

Recent Advances in Application of 1D Nanomaterials for Photocatalytic Nitrogen Fixation

Ragesh Nath R.¹, Shamkumar P. Deshmukh² , Sachin J. Kamble³  and Valmiki B. Koli^{1,4,*} ¹ Department of Physics, National Dong Hwa University, Hualien 97401, Taiwan; 810814307@gms.ndhu.edu.tw² Department of Chemistry, Damani Bhairuratan Fatechand, Dayanand College of Arts and Science, Solapur 413002, MS, India; spdeshmukh@dayanandsolapur.org³ Sanjay Ghodawat Institute, Atigre, Kolhapur 416118, MS, India; sachin.kamble@sgipolytechnic.in⁴ School of Nanoscience and Biotechnology, Shivaji University, Kolhapur 416004, MS, India

* Correspondence: valmikikoli12@gmail.com

Abstract: Ammonia, as the second most-produced chemical worldwide, serves diverse roles in the industrial and agricultural sectors. However, its conventional production via the Haber–Bosch process poses significant challenges, including high energy consumption and carbon dioxide emissions. In contrast, photocatalytic nitrogen (N₂) fixation, utilizing solar energy with minimal emissions, offers a promising method for sustainable ammonia synthesis. Despite ongoing efforts, photocatalytic nitrogen fixation catalysts continue to encounter challenges such as inadequate N₂ adsorption, limited light absorption, and rapid photocarrier recombination. This review explores how the electronic structure and surface characteristics of one-dimensional nanomaterials could mitigate these challenges, making them promising photocatalysts for N₂ fixation. The review delves into the underlying photocatalytic mechanisms of nitrogen fixation and various synthesis methods for one-dimensional nanomaterials. Additionally, it highlights the role of the high surface area of one-dimensional nanomaterials in enhancing photocatalytic performance. A comparative analysis of the photocatalytic nitrogen fixation capabilities of different one-dimensional nanomaterials is provided. Lastly, the review offers insights into potential future advancements in photocatalytic nitrogen fixation.



Citation: Ragesh Nath R.; Deshmukh, S.P.; Kamble, S.J.; Koli, V.B. Recent Advances in Application of 1D Nanomaterials for Photocatalytic Nitrogen Fixation. *Nitrogen* **2024**, *5*, 349–372. <https://doi.org/10.3390/nitrogen5020023>

Academic Editors: Jie Li, Adnan Mustafa and Jan Frouz

Received: 9 February 2024

Revised: 9 April 2024

Accepted: 15 April 2024

Published: 22 April 2024



Copyright: © 2024 by the authors. Licensee MDPI, Basel, Switzerland. This article is an open access article distributed under the terms and conditions of the Creative Commons Attribution (CC BY) license (<https://creativecommons.org/licenses/by/4.0/>).

Keywords: photocatalysis; nitrogen fixation; 1D nanomaterials; active sites

1. Introduction

Ammonia (NH₃) is essential for sustaining life on Earth, serving as a crucial component of nitrogen fertilizers and a primary ingredient in various chemical products such as nitric acid and explosives. It is also valued for its high hydrogen storage capacity, making it an eco-friendly material. With an estimated global production of approximately 15 billion metric tons annually, the demand for ammonia is expected to rise with continuing economic and population growth [1]. Presently, the Haber–Bosch process is widely utilized for the synthesis of industrial ammonia. However, the Haber–Bosch process mandates operating conditions exceeding 200 bars in pressure and temperatures surpassing 673 K. Additionally, a substantial quantity of H₂ generated by the steam reforming of fossil fuels must be combusted. Approximately 13% of the global oil supply and 35% of the global natural gas supply are allocated to specific regions. The feasibility of ammonia synthesis under normal atmospheric conditions, without the use of hydrogen gas, presents an attractive alternative for secure and environmentally sustainable production. Utilizing nitrogen directly at normal temperature and pressure can result in substantial energy savings, as the atmosphere contains approximately 78% nitrogen resources [2]. Under favorable circumstances, photocatalysis has the potential to convert nitrogen gas into ammonia. The initial investigation of photocatalytic nitrogen fixation by Schrauzer and Guth in 1977 demonstrated the reduction of nitrogen to ammonia using iron (Fe)-doped titanium dioxide

(TiO₂) [3]. Remarkably, the solar energy incident on the Earth's surface within a single hour is capable of satisfying global energy demands for a full year. The utilization of photocatalytic nitrogen fixation is increasingly becoming a prominent area of interest. Photocatalytic nitrogen fixation operates at relatively low temperatures and pressures, utilizing solar energy to generate electrons and holes that subsequently react with water protons to reduce N₂ to NH₃ [4]. Semiconductors facilitate photon absorption in the process of photocatalysis, generating electron–hole pairs that drive oxidation–reduction reactions. When the energy of the incident light equals or exceeds the band gap of semiconductor nanoparticles, electrons in the valence band are compelled to transition into the conduction band. As a result, there is a scarcity of available holes in the valence band. This phenomenon gives rise to the generation of electron–hole pairs. Nanomaterials exhibit a multitude of defects and dangling bonds, which have the capability to confine electrons or holes, thereby impeding the recombination of these electrons and holes. The presence of trapped electrons and holes on the particle surfaces leads to the generation of a robust redox potential. The three main stages commonly observed in photocatalytic reactions are light absorption, charge carrier separation, and surface reduction, as illustrated in Figure 1.

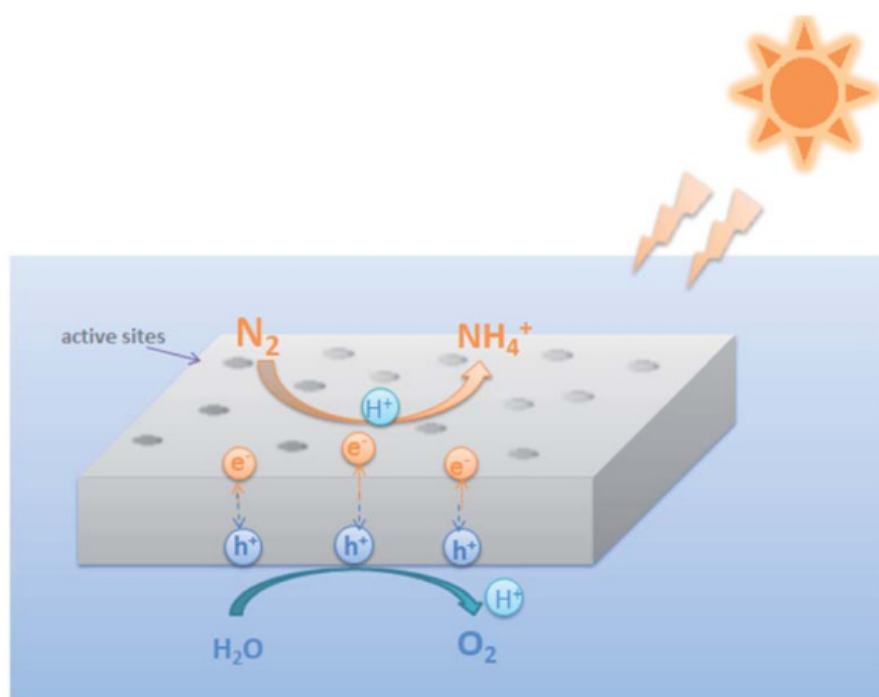


Figure 1. Plausible photocatalytic nitrogen fixation mechanism by photoactive nanomaterials [1]. Copyright 2021 Royal Society of Chemistry.

Despite the potential of common photocatalysts such as titanium oxide (TiO₂), zinc oxide (ZnO), graphitic carbon nitride (g-C₃N₄), and bismuth halides (BiOX), their nitrogen fixation efficiency remains low due to issues such as light absorption range and charge carrier recombination [5–7]. Recent studies have focused on modifying these materials to alter semiconductor band gaps, promote the separation of photogenerated electron–hole pairs, and enhance N₂ adsorption on the catalyst surface through methods such as doping, [8] constructing heterojunctions, and increasing vacancies [9]. This review extensively explores photocatalytic nitrogen fixation, synthesis methods of one-dimensional (1D) nanomaterials, and their applications in photocatalytic nitrogen fixation.

2. Overview of Semiconducting Nanomaterials for Photocatalytic N₂ Fixation

Materials with thickness and width on the nanoscale, such as nanorods, nanowires, nanoribbons, nanotubes, etc., are referred to as 1D nanostructures. They may have a length

of several microns or greater [10]. One-dimensional nanostructures with a high aspect ratio facilitate photogenerated carrier separation and transit more quickly, hence enhancing photocatalytic activity. Consequently, significant research has been conducted on how the design of 1D nanostructures affects photocatalytic nitrogen fixation. Photocatalytic nitrogen fixation, the process of utilizing a photocatalyst to reduce N_2 into ammonia under solar light irradiation, has garnered significant interest, with publications on the subject increasing 90-fold in just seven years [11]. For instance, the significance of the rutile phase of TiO_2 in photocatalytic N_2 reduction has been attributed to its strong chemisorption of N_2 on its surface [12]. The decline in photocatalytic N_2 reduction activity can be linked to the loss of Ti–OH groups and active sites within the rutile phase, particularly when the rutile-to-anatase phase ratio exceeds 23:77. Researchers have also examined the impact of incorporating metal oxides, such as Fe, Co, Mo, and Ni-based oxides, on the photocatalytic reduction of N_2 [13,14]. They found that the most favorable outcome in terms of ammonia generation occurred when Fe_2O_3 was added at a mass loading of 0.2 weight percent.

In 2017, Hirakawa et al. made a significant assertion that TiO_2 , with a substantial number of surface oxygen vacancies, exhibits catalytic activity in the conversion of N_2 to NH_3 under UV light, attributed to the creation of Ti^{3+} states. This leads to a remarkable enhancement in the efficiency of solar-to-chemical energy conversion in the photocatalytic N_2 reduction system, reaching 0.02%. This achievement establishes it as the most efficient photocatalytic N_2 reduction system to date [15]. In an intriguing study, Wang et al. generated self-assembled, 5 nm diameter Bi_5O_7Br nanotubes that exhibited high efficiency and stable N_2 photo fixation without requiring the use of a sacrificial agent [16]. It has been demonstrated that N_2 can be captured and activated by oxygen vacancies (OVs) on the surface of bismuth oxybromide-based photocatalysts, but these OVs are quickly oxidized. The process of synthesis and the mechanism of development of the Bi_5O_7Br nanotubes involved creating ordered bismuth-bromine-oleylamine (Bi-Br-OA) complexes. Initially, Bi and Br ions were coordinated in a pure oleylamine solution. Subsequently, the Bi-Br-OA compounds slowly hydrolyzed and self-assembled into a nanotube structure upon the gradual addition of water. The N_2 photo fixation of 5 nm Bi_5O_7Br nanotubes is divided into four steps: (i) Some oxygen atoms escape from the surface in the form of O_2 molecules to create abundant surface oxygen vacancies (OVs) under visible light; (ii) N_2 is chemisorbed and activated at the OV sites; (iii) The photogenerated electrons are injected into the activated N_2 molecule and reduced to NH_3 ; (iv) Finally, light-induced OVs can be easily restored to their original, stable OV-free state by adsorbing oxygen atoms from water and refilling them. To facilitate the emergence of unsaturated metal atoms and oxygen vacancy (OV) defects, which may be utilized as sites for N_2 chemisorption and electron transfer, Xiong's research group used $W_{18}O_{49}$ ultrathin nanowires as a model photocatalyst for complex Mo doping [17].

In addition to titanium dioxide, various other metal oxides, including iron (III) oxide (Fe_2O_3), zinc oxide, tungsten trioxide (WO_3), vanadium pentoxide (V_2O_5), and zirconium dioxide (ZrO_2), have demonstrated exceptional photocatalytic properties for nitrogen fixation. Additionally, certain metal sulfides, such as cadmium sulfide (CdS), have also exhibited promising catalytic capabilities in this regard [18,19]. Nevertheless, due to the susceptibility of the majority of these compounds to photodegradation, their production of ammonia is rather limited. Additionally, catalysts based on bismuth have exhibited noteworthy levels of activity in the process of photocatalytic reduction of N_2 [20,21]. The metastability of trapped photogenerated electrons on oxygen vacancies is crucial for the conversion of NH_3 , as it enables access to the π antibonding orbitals of activated N_2 molecules. Comprehending the intricate mechanisms governing nitrogen fixation is pivotal for optimizing its efficiency, offering invaluable insights into the underlying principles of the process. Presently, nitrogen fixation encompasses three primary mechanisms, collectively contributing to four recognized pathways: dissociative, distal associative, alternate associative, and enzymatic routes [22]. The dissociative pathway depicted in Figure 2a employs significant energy to effectively cleave the triple bonds present in nitrogen molecules. This process

subsequently leads to hydrogenation and the synthesis of ammonia [23]. The dissociative pathway is the mechanism through which ammonia is generated in the Haber process. The hydrogenation process exhibits distinct variations in the two associative pathways due to the gradual dissociation of the $\text{N}\equiv\text{N}$ bond. The process of hydrogenation initiates at the nitrogen atom that is located at the greatest distance from the catalyst, as depicted in the distal associative pathway illustrated in Figure 2b. Subsequently, the second nitrogen atom undergoes a hydrogenation process, resulting in the liberation of the first ammonia molecule. In the alternate associative approach depicted in Figure 2c, the hydrogenation of the two nitrogen atoms occurs simultaneously. Hydrogenation commonly occurs inside nitrogenases and other catalyst-mediated reactions in the enzymatic pathway, as depicted in Figure 2d. In contrast to the aforementioned approaches, the adsorption of the nitrogen molecule occurs on the nitrogenases or catalysts situated along the periphery of each atom, as opposed to being confined to a single atom's surface. In this process, the hydrogenation of each nitrogen atom occurs concurrently.

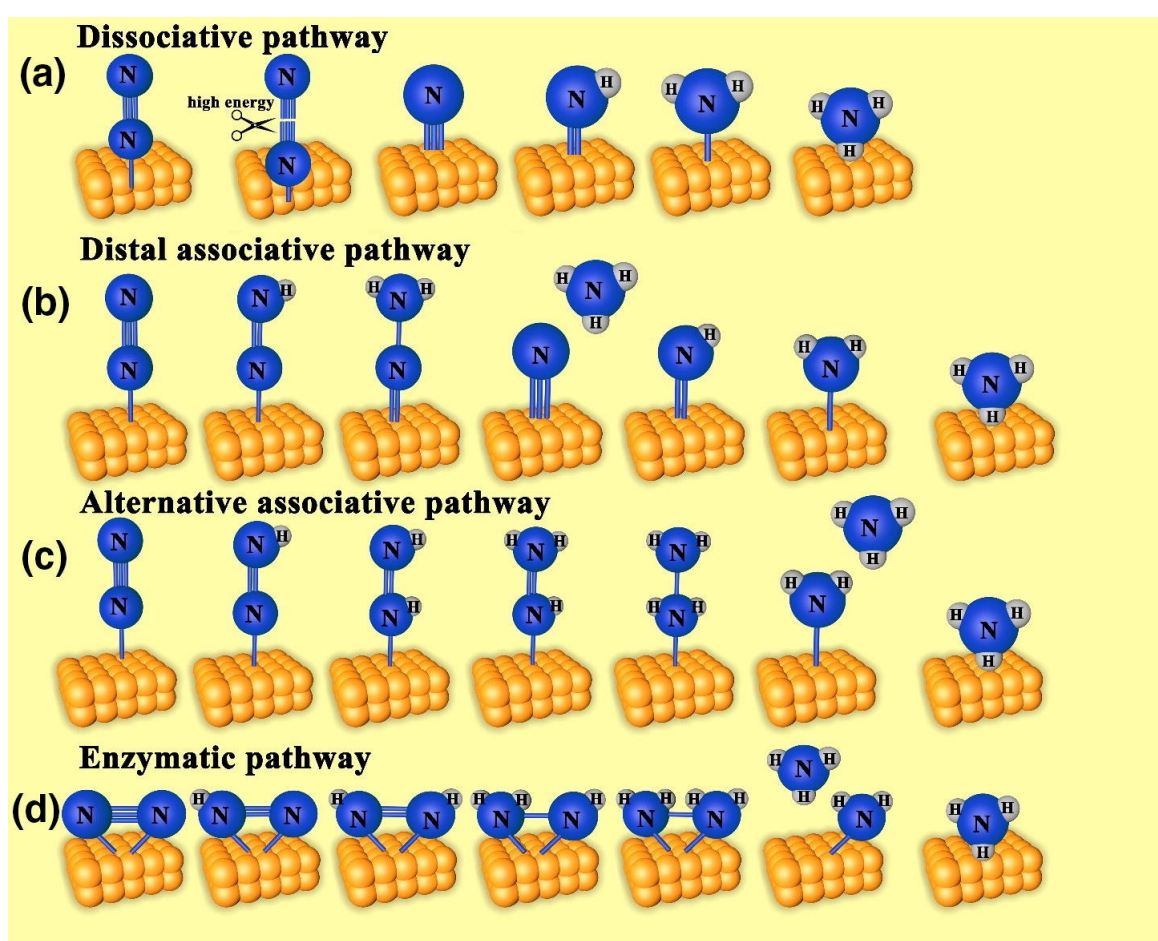


Figure 2. The pathways of nitrogen fixation to ammonia: (a) dissociative, (b) distal associative, (c) alternative associative, and (d) enzymatic. Reused with permission [24]. Copyright 2021 Elsevier.

In 2019, Ling et al. proposed a novel method for nitrogen reduction, termed surface hydrogenation, which is postulated to occur on the surface of metal catalysts based on noble metals Figure 3 [25]. The first phase of this mechanism involves the conversion of H^+ into $^*\text{H}$ with minimal energy. This is hypothesized to have potentially served as the rate-determining step. Subsequently, nitrogen molecules promptly undergo a reaction with hydrogen (H) to produce a more energetically favorable species, namely dinitrogen hydride (N_2H_2). Ammonia is formed by the reaction of N_2H_2 , H^+ , and electrons (e^-). Increasing

the concentration of alkali-metal cations can potentially serve as a viable way to accelerate the nitrogen fixation process, as they exhibit analogous behaviour to H^+ in activating N_2 .

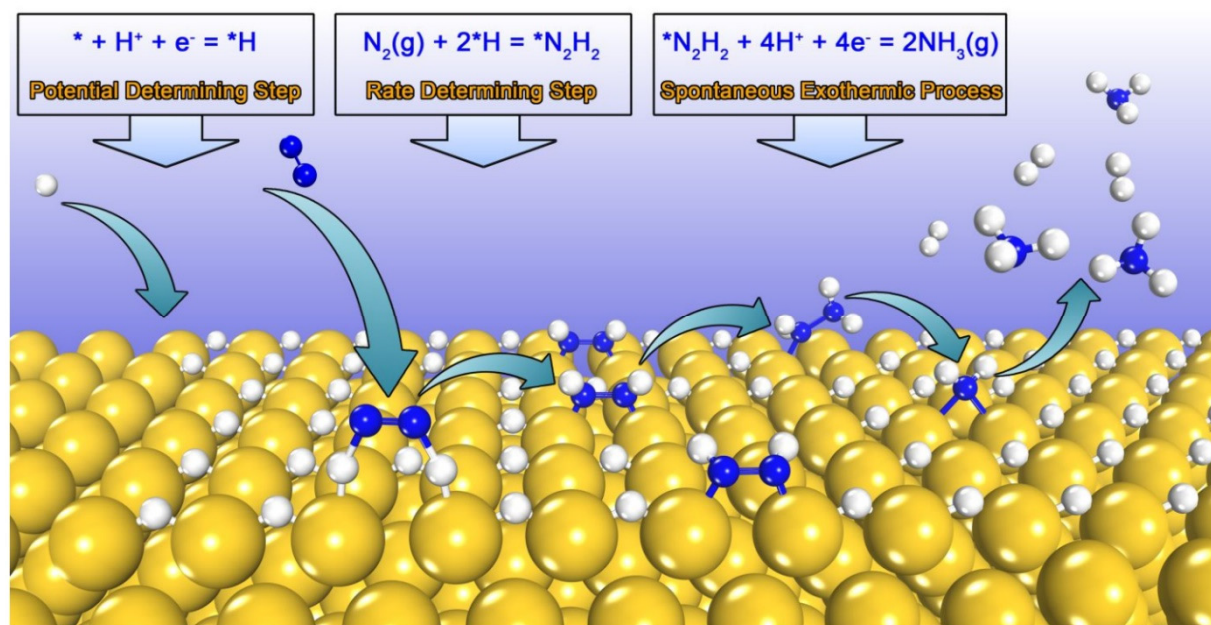
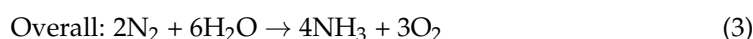


Figure 3. Noble-metal catalyst surface-hydrogenation mechanism for nitrogen reduction reaction (NRR). Potential determination begins with H^+ reduction into $*H$. N_2 molecules can overcome a high energy barrier to react with surface $*H$ to form $*N_2H_2$ intermediates as $*H$ coverage increases. This stage is crucial for establishing the overall process rate. $*N_2H_2$ spontaneously reduces to NH_3 after formation [25]. Copyright 2019 American Chemical Society.

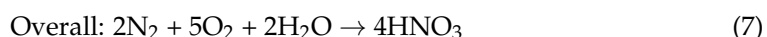
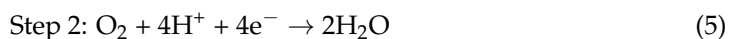
Mechanism of Photocatalytic N_2 Fixation

The photocatalytic nitrogen fixation process manifests through two distinct pathways: the nitrogen reduction reaction (NRR) and the nitrogen oxidation reaction (NOR). The process of N_2 reduction involves several sequential steps, which are delineated as follows: Initially, upon exposure to sunlight, photons generate electrons that become excited to the conduction band (CB), creating vacancies in the valence band (VB). Simultaneously, the formation of additional photo-induced holes (h^+) during electron-hole recombination catalyzes the oxidation of water, yielding H^+ and O_2 (Equation (1)). Subsequently, the energetic electrons facilitate the reduction of N_2 , yielding NH_3 (Equation (2)). NH_3 synthesis then occurs under standard temperature and pressure through the combination of water and N_2 , with sunlight serving as the primary energy source (Equation (3)).

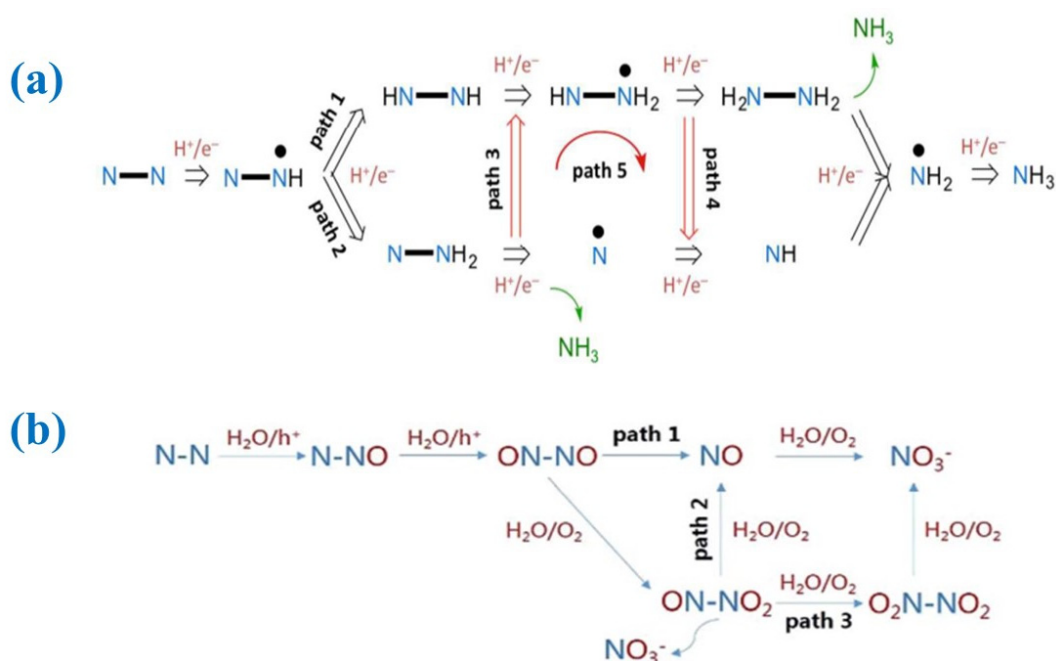


In the aforementioned illustration, it has been established that the photocatalytic process of N_2 oxidation adheres to the mechanism of photogenerated-hole oxidation. This process involves the following stages: First, when exposed to sunlight, electrons generated by photons get excited and move to the conduction band, creating holes in the valence band. The described behavior occurs within the nitrogen reduction reaction scenario. In this process, N_2 is oxidized to NO by the photogenerated h^+ in the presence of water (Equation (4)). At the same time, photoexcited electrons convert O_2 to H_2O (Equation (5)). Additionally, NO undergoes further oxidation to form nitrates, which serve as the final product (Equation (6)). Generally, the synthesis of nitric acid involves the combination

of water, oxygen (O_2), and nitrogen (N_2) under standard temperature and pressure. This process is facilitated by the utilization of sunlight as an energy input, as represented by (Equation (7)).

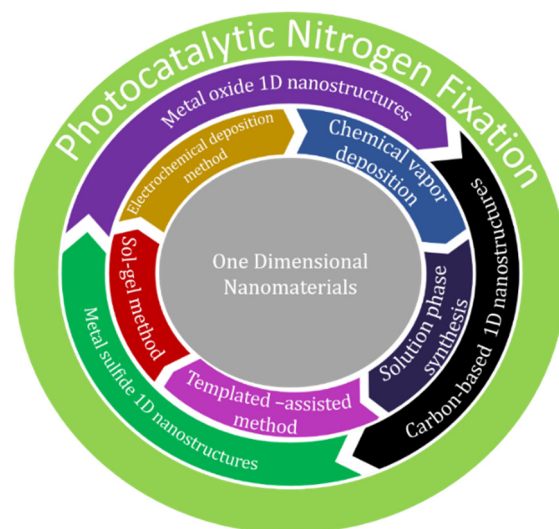


Adsorption sites can include individual atoms or specific locations within a group of atoms. However, defect sites also can adsorb reactant molecules and are generally more active in facilitating crucial photocatalytic reactions. In practical applications, there are five potential reaction pathways for photocatalytic N_2 reduction and three potential reaction pathways for photocatalytic N_2 oxidation. These pathways are visually depicted in Scheme 1a,b. The photocatalytic N_2 reduction reaction can be categorized into two distinct pathways: the associative alternating route and the associative intermediate pathway [26].



Scheme 1. (a) Five proposed routes for the photocatalytic N_2 reduction reaction mechanism [26]. Copyright 2016 Royal Society of Chemistry. (b) Three proposed routes for the photocatalytic N_2 oxidation reaction mechanism [27]. Copyright 2019 Royal Society of Chemistry.

In the realm of scientific literature, a diverse array of nanomaterials with varied morphologies have been utilized to advance photocatalytic nitrogen fixation. These include nanoparticles, nanosheet nanotubes, nanorods, and materials with zero-dimensional (0D), one-dimensional (1D), two-dimensional (2D), and three-dimensional (3D) structures. While extensive research has been conducted on nanomaterials with 0D, 2D, and 3D architectures for nitrogen fixation, exploration of 1D nanomaterials in this domain remains relatively limited, with scant scholarly discourse available. Consequently, the current literature predominantly focuses on the synthesis and application of one-dimensional nanomaterials in the realm of photocatalytic nitrogen fixation (See Scheme 2).



Scheme 2. Schematic illustration depicts various synthesis methods and functional one-dimensional nanostructures intended for potential applications in photocatalytic nitrogen fixation.

3. One-Dimensional (1D) Nanomaterials

One-dimensional semiconducting nanomaterials belong to an emerging class of semiconductors characterized by cross-sectional dimensions ranging from 1 to 100 nm and variable lengths spanning from hundreds of nanometers to millimeters. The foundation of today's research on 1D nanomaterials is based on Dr. R.S. Wagner's research in the 1960s at Bell Laboratories [28,29]. He developed a method called the 'vapor–liquid–solid process' for the synthesis of nanowires (specifically, silicon nanowires) on gold catalysts. By the 1990s, interest had shifted mainly to the exploration of carbon nanotubes (CNTs) [30–32] and several oxide materials [33,34] and elemental semiconductors [35–37]. Among 1D nanomaterials, nanowires (NWs), nanobelts, nanofibers, nanotubes (NTs), and nanorods (NRs) possess unique and exceptional properties due to their confined dimensionality along one axis [38–41]. These properties distinguish them from bulk and one-dimensional materials and make them highly attractive for various applications. Additionally, their higher surface area, improved active surface sites, and fewer lattice defects are favorable for reducing electron–hole recombination in long-run electron transfer reactions [42,43]. These materials, characterized by their elongated and anisotropic structures, exhibit exceptional electrical, optical, mechanical, and catalytic properties, making them valuable in fields ranging from electronics and photonics to energy storage and sensing [42,44–46].

Nanomaterial for Photocatalytic N₂ Fixation

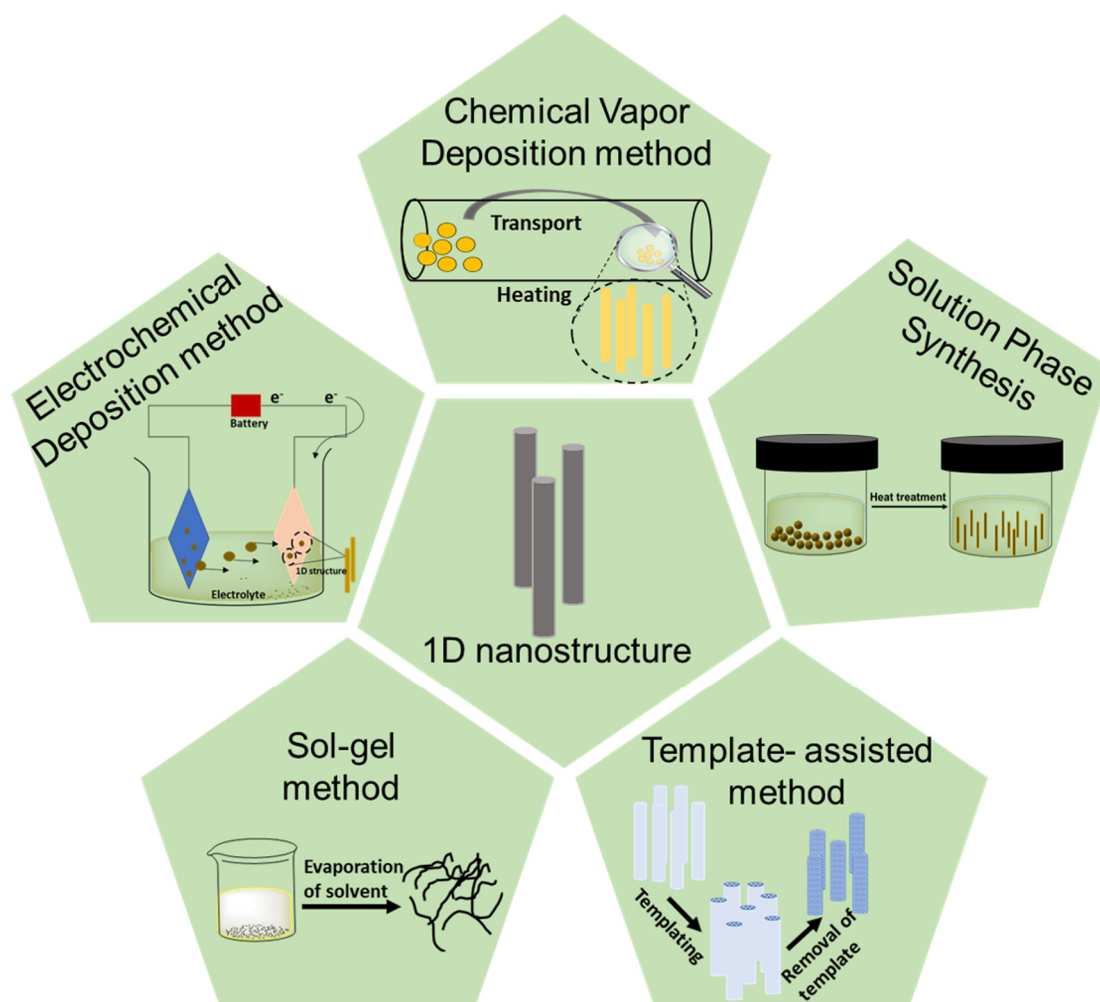
The potential of 1D nanomaterials in the area of heterogeneous photocatalysis is immense, especially following the invention of CNTs and TiO₂, which can function as single materials or be incorporated with other materials of various functionalities. As a result, 1D nanomaterials are becoming an active research topic, especially in solar water splitting, NH₃ conversion, organic dye degradation, photocatalytic nitrogen oxides (NO_x) removal, and photocatalytic N₂ fixation [47–50]. Similar to TiO₂ nanorods, zinc oxide exhibits similar 1D nanostructures with comparable band gap energies (3.2–3.3 eV), which exhibit higher reaction rates [51]. On the other hand, to maximize visible light absorption, narrow band gap semiconductors are used, either alone or coupled with sensitizers [52–54]. TiO₂ 1D nanostructures, such as nanorods or nanowires, exhibit enhanced photocatalytic efficiency in the N₂ fixation reaction [55]. The infusion of dopants or the fabrication of heterostructures with TiO₂ can significantly enhance its efficiency, often resulting in a substantial increase in performance [56,57]. Materials composed of noble metals with one-dimensional structures demonstrate efficient catalytic rates in photocatalytic N₂ fixation. However, the reaction kinetics in such systems may not meet the desired standards for optimal performance. To

improve the potential for enhanced efficiency, achieving effective charge transfer is crucial. One promising strategy involves assembling bimetallic or trimetallic compositions. This approach can significantly enhance charge transfer processes and prevent particle agglomeration on the surface, ultimately leading to improved catalytic performance [58–60]. $g\text{-C}_3\text{N}_4$, known for its two-dimensional sheet-like structure, is highly regarded for its eco-friendly, cost-effective, and metal-free semiconductor properties, making it suitable for a wide range of applications. However, its rapid recombination of electron–hole pairs poses a challenge, creating barriers for interplanar charge transfer and complicating its catalytic efficiency. To enhance catalytic performance, one strategy involves template-based methods or intricate synthesis routes to produce one-dimensional $g\text{-C}_3\text{N}_4$ structures. These one-dimensional configurations offer improved catalytic efficiency and more efficient charge transport along a single direction, mitigating the limitations associated with their 2D counterparts. Metal-organic frameworks (MOFs) have emerged as noteworthy antecedents and templates in the fabrication of one-dimensional nanostructures, which is an intriguing observation. This category of nanoparticles includes a diverse range of chemicals, such as metal phosphides, metal sulfides, porous carbon compounds, and metal oxides [61,62]. One noteworthy attribute of these derived materials is their ability to preserve the intricate pore structure inherited from the original MOF, giving rise to materials with elevated surface areas and distinctive structural characteristics. For instance, the creation of a porous hollow tubular In_2O_3 semiconductor, derived from the MIL-68(In) MOF, exemplifies this preservation. In their study, Hu et al. synthesized a photocatalyst consisting of In_2O_3 -decorated $g\text{-C}_3\text{N}_4$, generated from a Metal-Organic Framework (MOF) called MIL-68(In). The catalyst demonstrated remarkable efficiency in the process of photocatalytic hydrogen (H_2) production [63]. In a similar vein, Bariki et al. proposed the concept of utilizing MOF-derived hollow tubular heterostructures composed of $\text{In}_2\text{O}_3/\text{MIIIn}_2\text{S}_4$ (where MII represents calcium, manganese, and zinc) for photocatalytic applications such as hydrogen production, hydrogen peroxide (H_2O_2) production, and ammonia (NH_3) production [64]. Recently, metal doping with 1D W_xO_y (stoichiometric and non-stoichiometric) materials has become a promising photocatalyst for improving the N_2 fixation reaction. The incorporation of Mo, Ce, and Fe doping on $\text{W}_{18}\text{O}_{49}$ nanowires has been the subject of extensive research, showcasing the remarkable potential for improving the efficiency of N_2 fixation compared to conventional WO_3 materials [17,65,66]. It is widely acknowledged that one-dimensional nanostructures hold significant potential as fundamental components for developing advanced electrical or photoelectronic devices, chemical or biological sensors, and energy harvesting, storage, and conversion systems in the future [67]. Both descriptions are relevant to the physical and technological importance of one-dimensional nanostructures. Nevertheless, there has been limited focus on conducting extensive analyses of the potential practical applications of one-dimensional nanomaterials, which is of utmost importance for both scientific and industrial considerations. Therefore, considering the potential to address current deficiencies and issues related to energy and the environment, it is necessary to conduct more impartial and focused assessments on the potential practical applications of nanomaterials based on one-dimensional structures. In recent times, the use of one-dimensional nanostructures in photocatalysis, particularly in the context of nitrogen fixation, has emerged as a highly active research area within the nanoscience community. Nonetheless, there have been only a limited number of comprehensive reviews that have thoroughly examined the application of one-dimensional nanostructures in photocatalytic nitrogen fixation. The aforementioned circumstance serves as a compelling impetus for the composition of this feature article, which aims to present a comprehensive analysis of the noteworthy subject matter related to 1D-based photocatalysts used in photocatalytic nitrogen fixation.

4. Synthesis Methods for 1D Nanomaterials

The synthesis of one-dimensional nanomaterials is a critical aspect of harnessing their potential. Researchers have developed a wide array of synthesis techniques, each with its own advantages and limitations, to produce these nanoscale wonders. Two primary

approaches are employed in the synthesis of nanomaterials: bottom-up and top-down methods. Bottom-up methods involve building nanoscale structures from individual atoms or molecules, while top-down methods involve reducing larger materials to nanoscale dimensions. Of the two, bottom-up methods have gained widespread popularity due to their precision and control in creating tailored 1D nanostructures. In this brief section, we will explore some of the commonly employed synthesis methods in Scheme 3, and highlight their significance in tailoring the properties of one-dimensional nanostructures.



Scheme 3. Illustration of different synthesis methods for 1D nanostructures.

4.1. Chemical Vapor Deposition Method

The high-temperature vapor-phase synthesis technique is extensively employed for the production of one-dimensional nanostructures, with a special emphasis on metal oxide materials. Several scientific journals have conducted research on this well-established approach. The chemical reaction involves the combination of metal vapor with an oxidizing gas, such as oxygen or nitrogen, in a direct and uncomplicated manner. In a conventional vapor-phase synthesis method, the reaction takes place within a horizontally oriented quartz tube positioned within a furnace operating at elevated temperatures. The interior of the tube is used for loading the raw material, specifically metal powder, which is placed into an alumina boat and then injected upstream. A substrate is positioned downstream to accumulate the ultimate product.

(a) Direct vapor synthesis

In the direct vapor-phase synthesis process, both the metal and the oxidizing agent are introduced into the reaction chamber. The metal is then heated to the vapor phase and

undergoes a reaction with the oxidizing agent. The major governing factor in synthesizing one-dimensional nanostructures via the vapor phase is supersaturation, also known as metal vapor pressure. To facilitate the creation of 1D nanostructures, maintaining a low degree of supersaturation is imperative. Conversely, medium supersaturation is required for the growth of bulk crystals, while high supersaturation is necessary for powder growth and the membrane-based synthesis of nanomaterials. There are two distinct methods for vapor-phase growth: vapor–liquid–solid (VLS) and vapor–solid (VS). The VLS approach is a growth technique that utilizes metal nanoparticles as nucleation seeds. The growth direction and diameter of resulting one-dimensional nanostructures are controlled using the vapor–liquid–solid (VLS) approach. The process begins with the generation of liquid alloy droplets, comprising a combination of metal and a catalyst. As the experimental procedure progresses, the liquid alloy undergoes a state of supersaturation due to the accumulation of the desired metal vapor. Metal oxide is produced through gas oxidation, where oxidizing gases such as oxygen are introduced and allowed to flow. TEM examination has confirmed the presence of a catalyst nanocluster located near the end of the one-dimensional nanostructure, which is a notable characteristic of the VLS process [68,69]. For instance, two different catalysts, namely Au and Fe, could be employed for the synthesis of silicon nanowires. According to the Au–Si binary system phase diagram depicted in Figure 4, it can be inferred that nanowire formation is expected to occur at temperatures slightly above 363 °C. This temperature is notably more than 800 °C lower compared to the Fe-based catalyst.

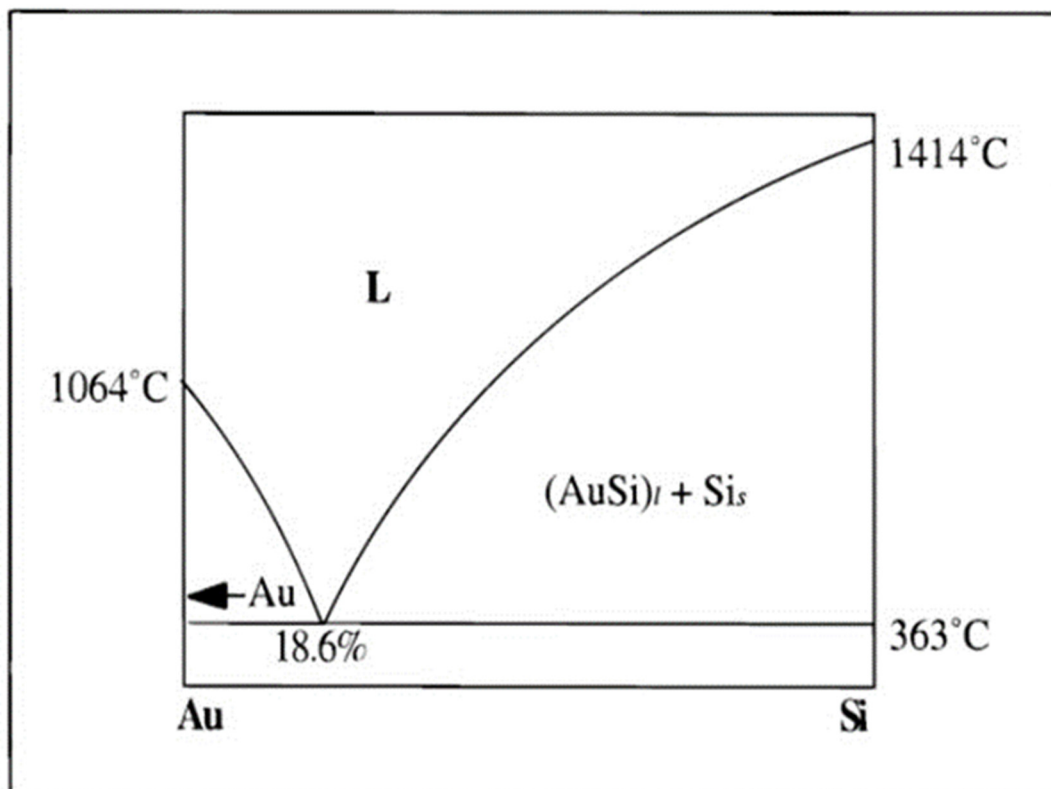


Figure 4. Phase diagram of Au-Si binary system [33]. Copyright 1999 American Chemical Society.

(b) Indirect vapor phase synthesis

The indirect vapor-phase synthesis technique is commonly employed for the growth of one-dimensional nanostructures. In this process, intermediates or precursors are typically involved. Due to the need to account for breakdown and other forms of side reactions in various scenarios, the synthesis method employed in this approach is more complex compared to the relatively straightforward chemical vapor deposition (CVD) process. In their

study, Yang et al. presented a technique for producing magnesium oxide (MgO) nanowires using a carbon thermal reduction process. Initially, a chemical reaction is initiated between carbon and MgO to facilitate the conversion of MgO into Mg vapor. The Mg vapor is then transported onto the surface of the condensation substrate, where it undergoes oxidation to regenerate MgO [70]. One notable benefit of employing the two-step process is the effective control of Mg vapor supersaturation through the reaction rate between MgO and carbon. This level of control facilitates the formation of one-dimensional MgO nanowires. An alternative technique for indirect vapor-phase development is metal–organic chemical vapor deposition (MOCVD), wherein the source metal is supplied through the utilization of metal-organic compounds [71]. The laser ablation method exhibits similarities to the chemical vapor deposition growth process. There are differences in the way in which they generate metal vapor. In the latter method, metal vapor is generated by laser ablating a metal component, which rapidly transitions the metal to the vapor phase inside the chemical vapor deposition process. The growth mechanism of laser ablation remains rooted in the vapor–liquid–solid or vapor–solid process [72].

4.2. Solution Phase Synthesis

The growth of solution-phase synthesis requires significantly lower temperatures compared to vapor-phase synthesis, resulting in a decrease in the overall cost of synthesis. The process of solution-phase synthesis can be strategically planned to facilitate the synthesis of a wide range of materials. These materials encompass several types, including elemental substances like gold and platinum, binary compounds such as TiO₂, ZnO, and CdTe, as well as complex compounds like barium titanate (BaTiO₃) and magnesium hydroxide sulfate hydrate [73–76]. In contrast, vapor-phase synthesis is restricted to fundamental materials, specifically metal elements or combinations of metal binaries. This approach has effectively achieved the synthesis of many morphologies. Coprecipitation and hydrothermal methods represent a selection of solution-phase synthesis methods employed for the fabrication of one-dimensional nanomaterials.

(a) Coprecipitation

The phenomenon of coprecipitation encompasses a series of sequential stages, including nucleation, growth, and coarsening. The complexity of the phases involved in coprecipitation has hindered the development of a comprehensive understanding of this phenomenon. Nevertheless, the subsequent content provides a fundamental outline of the procedure:

- (1) Typically, the solubility of desired products in a specific solvent is limited.
- (2) Supersaturation is a determinant factor that influences the growth of a product.
- (3) Elevated supersaturation levels induce the process of nucleation, leading to the creation of a significant quantity of clusters or nuclei.
- (4) The crystals undergo development into larger structures as ions or molecules are introduced.
- (5) The size and morphology of the final result can be significantly influenced by secondary growth mechanisms, such as Ostwald ripening or aggregation.

The coprecipitation method has been used to fabricate various nanoparticles, including elemental metal and metal oxide. For instance, Zagari et al. synthesized ZnO nanorods using this process. They sensitized the nanorods with tetrakis(4-carboxyphenyl) porphyrin and its tin complex to enhance their visible light photocatalytic activity [77]. Soares et al. synthesized nanotube/nanorod-like structures of La-doped ZnO using the co-precipitation method for the degradation of methylene blue and ciprofloxacin [78]. Wang and colleagues developed a simple method using coprecipitation to create hierarchical microcuboids of CuBi₂O₄ by self-assembling nanorods. These materials have an average size of 6 μm in length and 1.5 μm in width. Additionally, modifying them with an AuAg alloy increased their photocatalytic efficiency by 1.9 times [79].

(b) Hydrothermal/Solvothermal synthesis

The solvothermal method utilizes supercritical fluids, which are fluids heated to temperatures and pressures above their boiling point, exhibiting characteristics of both liquids and gases. The reduction in interfacial tension leads to a significant improvement in mass movement between phases. When water is the solvent, the process is often referred to as hydrothermal. If an organic solvent is used, then the process is termed solvothermal. Although some syntheses have been conducted under supercritical conditions, the vast majority of nanomaterial synthesis occurs at significantly lower temperatures and pressures [80–82]. This approach has been used to create a variety of essential nanomaterials with 1D morphologies, such as nanotubes, nanorods, and nanowires, including TiO₂, ZnO, g-C₃N₄, and CdTe [80,83–85]. The hydrothermal approach has been extensively used for synthesizing nanostructured titania, which is considered a highly significant photocatalyst. Wangs and Ge groups conducted a comprehensive examination to investigate the effects of hydrothermal conditions on the growth of TiO₂ nanotubes [86,87]. The diameters of the nanotubes were found to depend on temperature and reactant ratio, with higher temperatures resulting in larger nanotubes with a wider size dispersion. Under hydrothermal conditions, some researchers utilized various acids as catalysts to transform amorphous TiO₂ into anatase or rutile crystallite TiO₂ [88]. Nanorods in the rutile phase can be synthesized using citric and nitric acid, while the conversion of amorphous TiO₂ to the anatase phase can be achieved by employing hydrofluoric acid.

4.3. Template Assisted Synthesis

Another method of synthesizing 1D nanostructures utilizes pre-existing nanostructures in a process known as ‘template synthesis’. Various templates have been utilized to create nanostructure materials, including polymeric membranes and self-assembled molecular structures [89,90]. The two most commonly used templates are polymers and anodic aluminum oxide (AAO). In the synthesis process, the AAO membrane, which has well-organized channels, is immersed in the reaction system. Subsequently, the reaction solution is subjected to electrochemical deposition within the pores of the AAO membrane. The required nanowires can then be obtained by dissolving the AAO membranes in NaOH solution [91,92]. Polymer materials can be used as templates due to their ease of processing. They can either serve as sacrificial templates or as guiding agents during the synthesis of hollow structures. Caruso described a method for producing hollow SiO₂ nanomaterials [93]. This methodology employed polystyrene spheres as templates, followed by coating SiO₂ particles onto their surfaces using poly(diallyl dimethyl ammonium chloride) (PDADMAC). Calcination then led to the formation of silica spheres with hollow interiors. Similarly, a core-shell structure consisting of silver and gold layers was fabricated using polystyrene as the core template [94]. Poolakkandy et al. developed an easy method for synthesizing transition metal oxides that allows for precise morphological (1D, 2D, and 3D) and physicochemical control [95].

4.4. Sol-Gel Method

One-dimensional nanostructures with a porous membrane have been produced using the sol-gel synthesis process [96]. The sol-gel technique relies on a gel composed of aggregated sol particles. A membrane template is submerged in the sol suspension, causing sol aggregates to form on its surface. These sol particles fill the template’s pores, creating nanostructures with a high aspect ratio. The deposition period determines the length of the nanostructures. Finally, the gel is removed through a heating process, completing the production of desired nanostructures, such as one-dimensional arrays of gold (Au), ZnO nanorods, and MnO₂ nanowires [97,98]. Matysiak et al. synthesized hybrid amorphous/crystalline SnO₂ 1D nanostructures and studied their shape, structure, and optical characteristics [99]. Reyes et al. used a simple route to obtain TiO₂ nanowires via the sol-gel method [100].

4.5. Electrochemical Deposition

The process of electrochemical deposition involves applying a metal coating to one side of the membrane, which acts as a cathode for electroplating within the pores. In other words, electrically conductive membranes with appropriate channels are used as templates for synthesizing nanowires via electrochemical deposition. Since cations in the deposition solution reduce at the cathode, they adhere to the template. The anode is placed parallel to the cathode in the deposition solution. When an electric field is applied, cations in the system diffuse towards the cathode, where they undergo reduction. This process leads to the formation of nanowires within the pores of the template. Electrochemical deposition is commonly used to synthesize metals, alloys, semiconductors, and electrically conductive polymers. This is facilitated by the fact that once the initial deposition occurs, the electrode becomes isolated from the precursor solution by the deposited materials. Consequently, the deposited material can serve as an electrically conductive substance, enabling it to function as a channel for electric current. The synthesis of nanostructures using this technology is primarily influenced by factors such as deposition duration, the length of the deposition channel or pore, and current density [101]. She et al. stated that electrodeposition is a straightforward and flexible approach for producing one-dimensional nanostructures, which has gained increasing attention in recent years [102].

5. Important 1D Nanostructures for N₂ Fixation

5.1. Metal Oxide 1D Nanostructures

Metal oxide nanostructures have garnered significant interest in the field of photocatalytic N₂ fixation due to their unique properties and potential to drive this challenging and important reaction. Indeed, various techniques and mechanisms have been developed for synthesizing one-dimensional metal oxide nanostructures. Some of the important nanostructures include nanotubes, nanowires, nanorods, and nanobelts. TiO₂ has emerged as a focal point in the study of oxide nanotubes due to its significant technological relevance. Researchers have increasingly turned their attention to TiO₂ for photocatalytic applications, drawn by its environmentally friendly properties, chemical inertness, and anisotropic behavior [103]. The pivotal development in creating tube-like structures for TiO₂ initially involved using anodic aluminum oxide templates and sol-gel techniques supported by supramolecular templates. However, its wide band gap (3.0–3.2 eV) and the increased recombination of photogenerated electrons and holes have led to reduced efficiency. To tackle these challenges, 1D TiO₂ nanostructures have been customized by combining them with other semiconductors or by introducing structural defects through the addition of metal or non-metal dopants. This innovation has led to augmented surface area, heightened efficiency, and superior absorption of visible light when compared to pure TiO₂ structures [104,105]. Wu et al. utilized a solvothermal synthesis method to fabricate TiO₂(B) nanotubes, employing MoO₃ nanorods as templates. These nanotubes demonstrated a notably larger surface area compared to pure TiO₂ nanosheets. Under natural sunlight, TiO₂(B) exhibited an NH₃ production rate of 106.6 μmol L⁻¹ g⁻¹·h⁻¹. This heightened activity can be attributed to improved charge separation and an increased presence of surface oxygen vacancies [106]. Similarly, Shufang et al. synthesized TiO₂ nanotubes adorned with Au nanocrystals, resulting in enhanced N₂ fixation performance along with excellent stability. SEM and TEM images of TiO₂ nanotubes and Au-decorated structures are presented in Figure 5. The presence of Au-decorated nanocrystals led to an augmentation of oxygen vacancies, enhancing the chemisorption of N₂ and promoting charge separation on the surface of TiO₂ nanotubes [107]. To mitigate surface defects on TiO₂ nanotubes, Wang and coworkers subjected the as-synthesized TiO₂ nanotubes to treatment with a H₂ atmosphere. This treatment yielded a remarkable NH₃ production rate of 1.2 mmol L⁻¹ g⁻¹·h⁻¹ under the full spectrum of light [55].

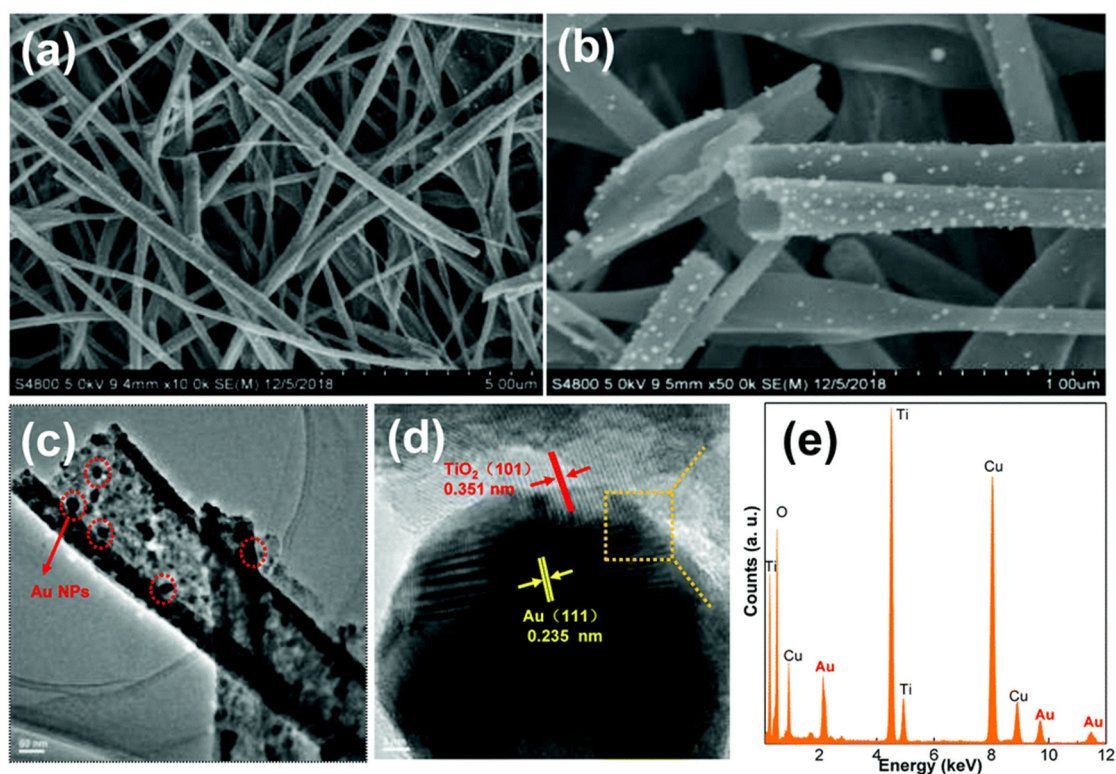


Figure 5. (a,b) Field emission scanning electron microscopy (FESEM) images of gold nanocrystals anchored TiO₂ nanotubes (Au@TiO₂ NT); (c) transmission electron microscopy (TEM) image of Au@TiO₂ NT. Gold nanocrystals are marked by dotted circles according to their darker contrast compared to TiO₂ nanotubes; (d) high-resolution TEM image of Au@TiO₂ NT. Lattice fringes are marked; and (e) energy-dispersive X-ray (EDX) spectroscopic analysis of the selected area (marked with a dotted square) in (d) [107]. Copyright 2020 Royal Society of Chemistry.

ZnO nanostructures have garnered significant attention, surpassing other semiconductor materials due to their ready availability and cost-effectiveness compared to known one-dimensional structures. ZnO primarily exists in three distinctive morphologies: nanotubes, nanorods, and nanowires [108]. ZnO nanowire-like structures started to be developed in the early 2000s through heating ZnO powders. TEM studies confirmed the formation of nanobelts, which usually have widths ranging from 50 to 300 nm [109]. In the same year, ZnO nanowires were successfully synthesized using a vapor transport method, resulting in diameters of 80–120 nm and lengths of 10–20 μm [108]. However, similar to TiO₂, ZnO nanostructures face challenges related to their wide band gap, which limits their efficiency in absorbing visible light. To address this issue, ZnO nanostructures have been fabricated in conjunction with other semiconductors and dopants, enabling efficient absorption of visible light. A recent breakthrough involved coupling ZnO nanorods with nickel phosphide (Ni₂P). Optimal loading of Ni₂P resulted in an impressive NH₃ production rate of 2304.43 $\mu\text{mol L}^{-1} \text{g}^{-1} \cdot \text{h}^{-1}$, a remarkable 3.3 times higher than that of the pure ZnO structure. The photocatalytic nitrogen fixation mechanism is shown in Figure 6 [110].

In addition to TiO₂ and ZnO nanostructures, scientists are also interested in studying one-dimensional nanostructures with different shapes and elements like tungsten oxide (W_xO_y), molybdenum oxide (Mo_xO_y), and bismuth oxide (Bi_xO_y). This helps improve their ability to absorb visible light for N₂ fixation. Among these, it is important to highlight tungsten oxide (W_xO_y) catalysts, which have recently emerged as crucial metal oxides for photocatalytic N₂ fixation. Among them, W₁₈O₄₉ stands out for its abundant oxygen vacancies, which can weaken the N \equiv N triple bond and enhance catalytic activity. Recently, Huan et al. reported the construction of asymmetric active sites on Ru/W₁₈O₄₉ via the hydrothermal method. The enhanced photocatalytic N₂ fixation is due to the synergistic

effect of Ru species with oxygen vacancies modifying the coordination to form Ru–O–W bonds. The reaction pathway for photocatalytic NH_3 generation is shown in Figure 7. The electrons produced as a result of the local surface plasmon resonance (LSPR) effect between Ru and oxygen species tend to reduce N_2 to NH_3 molecules [111]. Similarly, adding metals like Au, Fe, Mo, and Mn to $\text{W}_{18}\text{O}_{49}$, or combining it with other semiconductors like SbO_3 and $\text{g-C}_3\text{N}_5$, has shown impressive results in generating NH_3 through photocatalysis under visible light [65,111–113].

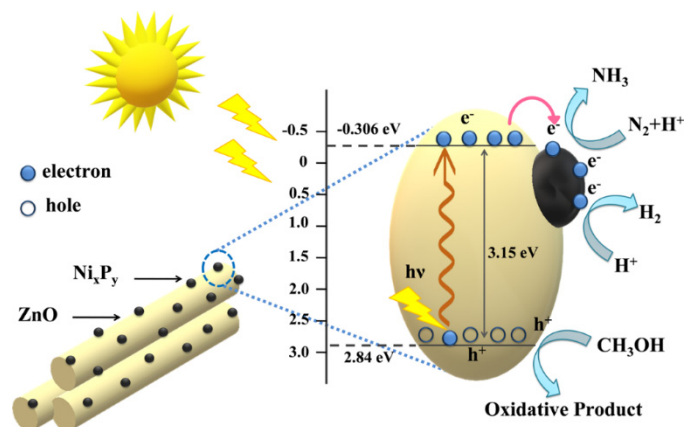


Figure 6. Schematic representation of the photocatalytic mechanism pathway illustrating charge separation and migration in the ZnO Ni_xP_y composite for solar light-assisted N_2 reduction and H_2 evolution [110]. Copyright 2021 American Chemical Society.

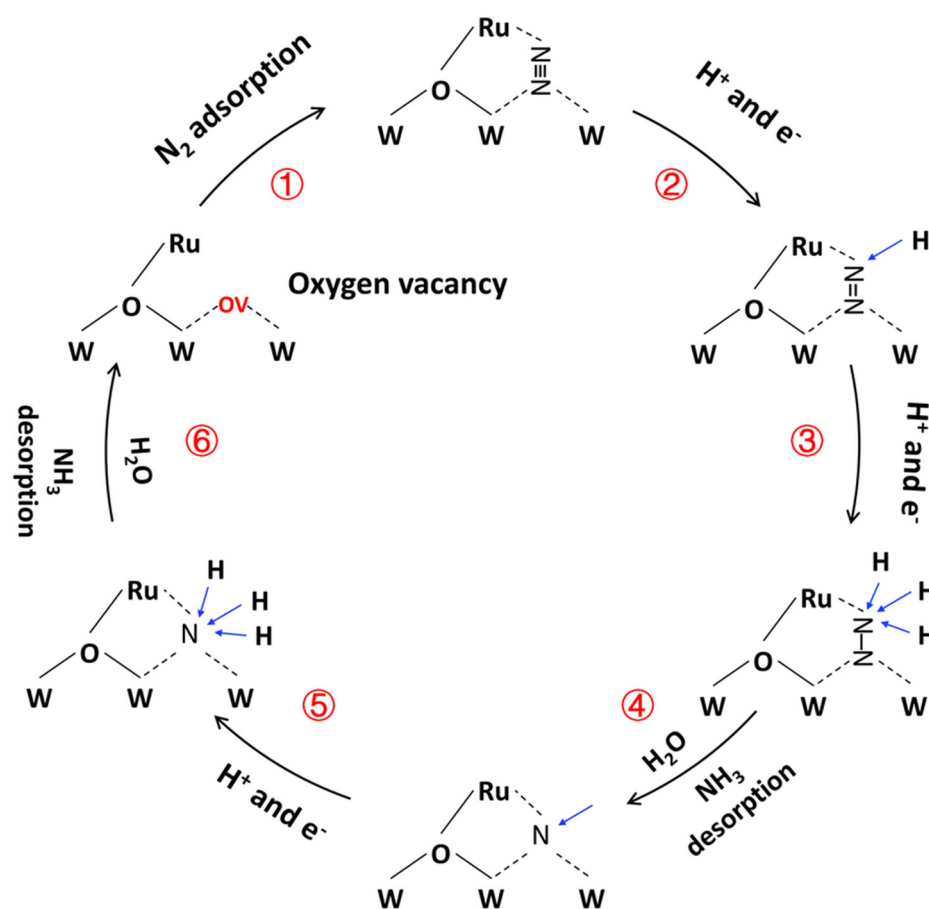


Figure 7. Proposed reaction pathway for photocatalytic N_2 fixation on $\text{Ru}/\text{W}_{18}\text{O}_{49}$ [114]. Copyright 2023 Royal Society of Chemistry.

5.2. Carbon-Based 1D Nanostructure

Carbonaceous one-dimensional nanostructures refer to carbon-based nanomaterials that exhibit a linear or rod-like shape, with the structure extending predominantly in one dimension. These materials have attracted significant attention due to their unique properties and versatile applications in various fields. Carbon nanotubes (CNTs), carbon nanofibers (CNFs), and carbon nitride materials (CNs) are prime examples of this class of material. Carbonaceous one-dimensional nanostructures have also been studied for their ability to catalyze N_2 fixation, which converts atmospheric nitrogen into ammonia or other nitrogen-containing compounds. Although carbon materials are not usually recognized for their inherent catalytic activity in N_2 fixation, they can act as supports or co-catalysts when combined with other materials. Ping Xing et al. conducted a comprehensive study on the impact of carbon-modified ZnO achieved through a hydrothermal process, followed by the photo-deposition of MoS_2 . In this context, carbon atoms function as a substrate material for loading both ZnO and MoS_2 . This composite, active under visible light, showed great performance in generating NH_3 through photocatalysis, reaching $245.7 \mu mol L^{-1} g^{-1} \cdot h^{-1}$, which is 9.3 times higher than pure ZnO. Adding carbon as a support material not only boosted the surface area but also improved charge separation effectively [115]. In a similar vein, a hybrid system comprising carbon-supported $WO_3 \cdot H_2O$ was found to exhibit significantly enhanced N_2 fixation capabilities compared to TiO_2 and Bi-OBr. This observation underscores the advantages of carbon decoration on tungstic acid, leading to improved charge transfer and separation in the catalytic process [116]. The presence of carbonaceous species can also act as a sacrificial agent that may directly react with atmospheric N_2 to form urea. To transform the morphology of the material, the water-induced method has been introduced, introducing water molecules into the substrate during the thermal process. For instance, Yijiao and colleagues synthesized nanoparticles of $NaYF_4:Yb,Tm$ (NYF) decorated on carbon nanotubes (CNTs). This combination showed the highest NH_3 production yield of $1.2 mmol L^{-1} gcat^{-1}$ when exposed to near-infrared light. Spectrochemical studies verified that NYF nanoparticles displaced the deep trap state and the edge of the conduction band. Moreover, these studies provided evidence that photogenerated electrons in nitrogen vacancy-free carbon nanotubes dissipate their energy by relaxing into multiple lower energy states [117]. Among carbon-based materials, carbon nitride stands out as a remarkable one-dimensional nanostructure for photocatalytic applications. This distinction is primarily attributed to its non-toxic nature and remarkable capacity to absorb visible light. Inspired by carbon nanotubes (CNTs), polymeric carbon nitride manifests in various morphologies, including nanowires, nanotubes, and nanorods. The material's specificity can be finely tailored by adjusting the synthesis methods [118,119]. A key advantage of the one-dimensional nanostructure of carbon nitride compared to its two-dimensional counterpart is its tubular structure. This structure improves the separation of photogenerated charge carriers and makes it easier for electrons to transfer along one direction in photocatalytic reactions [120,121]. Furthermore, $BiOBr_xI_{1-x}$ was coated on carbon nanofibers via electrospinning technology followed by a solvothermal method. Figure 8 illustrates the mechanism of photocatalytic N_2 fixation and Rhodamine B (RhB) degradation by $BiOBr_xI_{1-x}/CNF$. The optimal amount of bismuth oxyhalide with carbon nanofiber exhibited 85% photodegradation of tetracycline and a rate of $281 \mu mol L^{-1} g^{-1} \cdot h^{-1}$ for ammonia production. The $BiOBr_{0.6}I_{0.4}/CNF$ photocatalyst exhibited a 5.5-fold higher ammonia yield compared to pure $BiOBr_x$ [122].

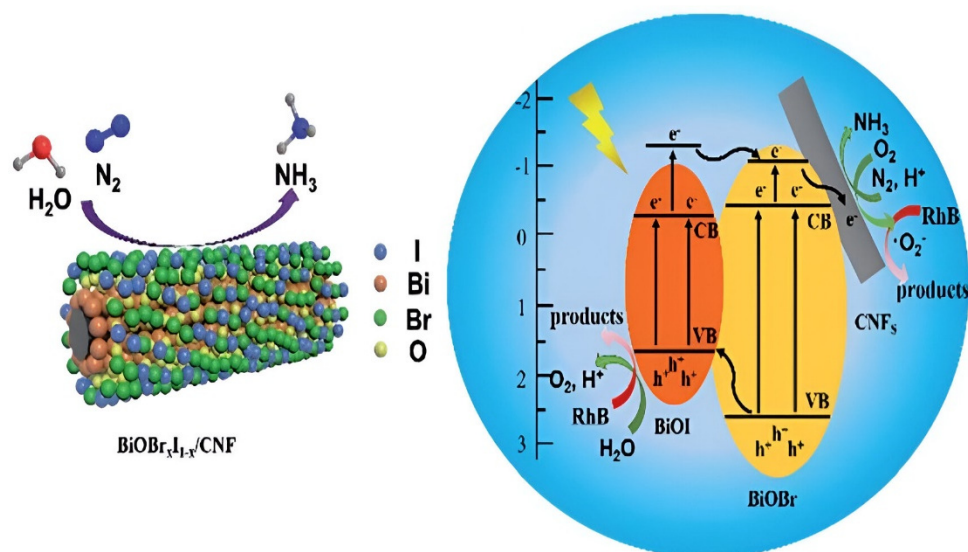


Figure 8. Mechanism for photocatalytic N_2 fixation and RhB degradation over the $BiOBr_xI_{1-x}/CNF$ [122]. Copyright 2020 Royal Society of Chemistry.

5.3. Metal Sulfide 1D Nanostructure

One-dimensional metal sulfide nanostructures consist of metal cations and sulfide anions arranged in a linear or rod-like fashion and have found diverse applications, including photocatalytic N_2 fixation. This is attributed to their unique properties, especially their smaller band gap and high photoelectric sensitivity compared to metal oxides, which traditionally suffer from wide band gaps. In the context of photocatalysis, the presence of sulfur vacancies, surface defects, and cationic vacancies plays a pivotal role in enhancing the photocatalytic efficiencies of metal sulfides (MS_x , where $x = 1, 2$). The synthesis of these one-dimensional metal sulfide nanostructures involves a range of techniques, including solvothermal methods, chemical vapor deposition, and hydrothermal processes, resulting in tunable properties that make them suitable for various applications. However, the application of 1D metal sulfide nanostructures in photocatalytic N_2 fixation has been comparatively less explored. One of the challenges in using metal sulfides as single photocatalysts is the rapid recombination of photogenerated electrons and holes due to their low band gap, which limits their photocatalytic efficiency. To address this limitation, He et al. introduced a novel approach by synthesizing In_2S_3 one-dimensional hollow structures specifically for photocatalytic N_2 fixation. They utilized an organic linker, MIL-68, as a precursor to create sulfur vacancies while maintaining the integrity of the one-dimensional structure. This innovative approach resulted in an enhanced NH_3 generation rate of $52.49 \mu\text{mol L}^{-1} \text{g}^{-1} \text{h}^{-1}$, surpassing that of the pure catalyst [123]. Among other metal sulfides, CdS has been well explored in photocatalytic applications. Sun et al. reported the synthesis of CdS nanorods on Ti_3C_2 MXene via a hydrothermal method. The nanocomposite material exhibited an excellent photocatalytic N_2 fixation rate of $293.06 \mu\text{mol L}^{-1} \text{h}^{-1}$ with an AQE of 7.88%. The material exhibited good stability under sunlight irradiation. The charge transfer from CdS to Ti_3C_2 MXene improved the ability to transfer charges. The presence of Ti_3C_2 reduces the migration distance of carriers and improves the shuttling of charge carriers between CdS and Ti_3C_2 . Similarly, materials like FeS_2 , NiS, CuS, and WS_2 are important metal sulfide materials that exhibit enhanced photocatalytic performance [124,125]. Tuning the surface properties by creating cation/anion vacancies can improve its photocatalytic efficiency in N_2 fixation rates. Apart from binary metal sulfides, ternary metal sulfides and composites also attract a lot of attention. Figure 9 represents the energy band structure and electron–hole separation of $ZnIn_2S_4$ @polyaniline ($PANI@ZnIn_2S_4$), as prepared by Chen et al. The transfer of conduction band electrons from PANI to $ZnIn_2S_4$ and vice versa for photogenerated holes improved NH_3 production to $290 \mu\text{mol L}^{-1} \text{g}^{-1} \text{h}^{-1}$ under visible

irradiation [126]. Details from the comparative study of various 1D nanomaterials with photocatalytic nitrogen production rate is shown in Table 1.

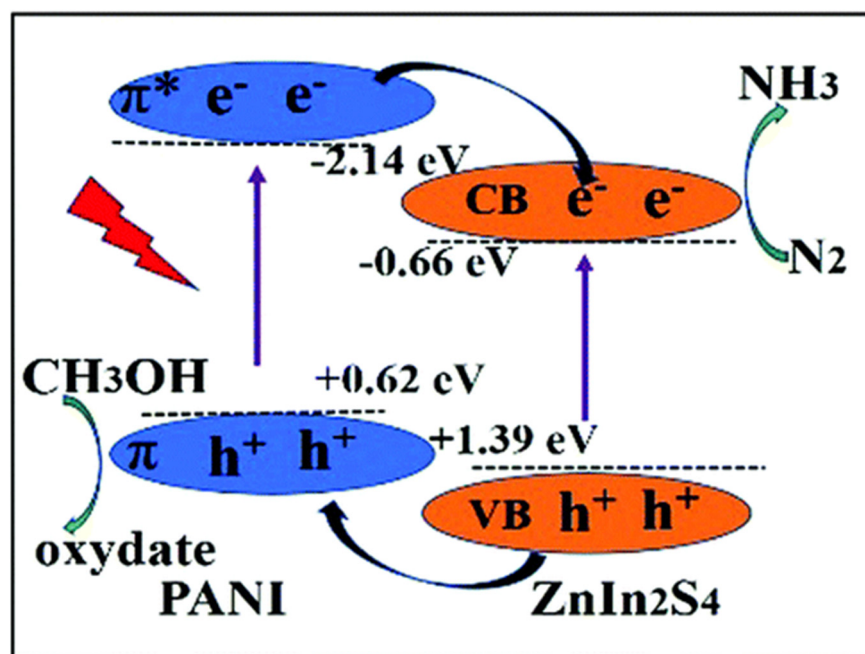


Figure 9. Schematic illustration of the energy band structure and charge separation of PANI@ZnIn₂S₄. Reproduced with permission from ref. [126]. Copyright 2020 Royal Society of Chemistry.

Table 1. One dimensional nanostructured photocatalyst for N₂ fixation.

SL No.	1D-Photocatalyst	Morphology	Light Source	Performance for Photocatalytic NH ₃ Generation	Reference
1.	TiO ₂ (B)	Nanotubes	300 Xe lamp (Sunlight)/ 300Xe lamp (full wavelength)	106.6 μmol g ⁻¹ / 318 μmol g ⁻¹	[106]
2.	TiO ₂	Nanotubes	300 Xe lamp (full wavelength)	1.2 mmol·L ⁻¹ ·h ⁻¹	[55]
3.	Au- TiO ₂	Nanotubes	500 W high-pressure mercury lamp	58.7 μmol g ⁻¹	[107]
4.	Bi ₅ O ₇ Br	nanotubes	300W Xe-lamp (>400 nm)	1.38 mmol g ⁻¹ h ⁻¹	[127]
5.	Mo- W ₁₈ O ₄₉	Nanowires	300 Xe lamp (full wavelength)	95.5 μmol g _{cat} ⁻¹ h ⁻¹	[128]
6.	Mn- W ₁₈ O ₄₉	Nanowires	300 W Xe-lamp (λ > 400 nm)	97.9 μmol g ⁻¹ h ⁻¹	[129]
7.	Ce- W ₁₈ O ₄₉	Nanowires	300 W Xe lamp (1500 mW/cm ²)	319.97 μg g ⁻¹ h ⁻¹	[66]
8.	Fe- W ₁₈ O ₄₉	Nanowires	Xe lamp (power density of 100 mW cm ⁻²)	375.2 μmol g ⁻¹	[65]
9.	Fe- W ₁₈ O ₄₉ /g-C ₃ N ₅	Nanowires	300 W Xe-lamp (simulated sunlight)	131.6 μmol g ⁻¹ h ⁻¹ ,	[111]
10.	W/Mo- W ₁₈ O ₄₉	Nanowires	300 Xe lamp (simulated sunlight)	184.54 μmol g ⁻¹ h ⁻¹	[130]
11.	Sb ₂ O ₃ @W ₁₈ O ₄₉	Nanowires	300 W xenon lamp (λ ≥ 420 nm)	600.1 μg h ⁻¹ g _{cat} ⁻¹	[113]

Table 1. Cont.

SL No.	1D-Photocatalyst	Morphology	Light Source	Performance for Photocatalytic NH ₃ Generation	Reference
12.	NaYF ₄ :Yb,Tm/g-C ₃ N ₄	Nanotubes	300 W Xe lamp (>420nm)	1.72 mmol L ⁻¹ g _{cat} ⁻¹	[117]
13.	CdS @Ti ₃ C ₂ MXene	Nanorod	300 W Xe-lamp (simulated sunlight)	293.06 μmol L ⁻¹ h ⁻¹	[131]
14.	In ₂ S ₃	nanotubes	300 W Xe-lamp (simulated sunlight)	52.49 μmol h ⁻¹ g ⁻¹	[123]
15.	PANI@ZnIn ₂ S ₄	Nanorods	visible light irradiation	290 μmol L ⁻¹ h ⁻¹	[126]
16.	1T-MoS ₂ /CdS	Nanorods	visible light, (780 nm > λ > 420 nm)	(8220.83 μmol L ⁻¹ h ⁻¹ g ⁻¹)	[132]

6. Conclusions and Outlook

It has been a century since the discovery and use of the Haber–Bosch method. Scientists have been exploring novel, gentler techniques for nitrogen fixation processes. Photocatalytic nitrogen fixation has the capability to utilize solar radiation to catalyze the reduction of atmospheric nitrogen molecules under favorable conditions. Despite the positive outcomes that generations of academics have obtained in recent years, industrial manufacturing of photocatalytic nitrogen fixation technology is still a long way off. The photocatalytic nitrogen reduction reaction requires the simultaneous fulfillment of three criteria by the photocatalyst: a high rate of light utilization, efficient separation of photogenerated electron–hole pairs, and a strong ability to adsorb and activate nitrogen molecules. There are several effective methods to enhance the aforementioned three needs, such as modifying the morphology of the material to introduce surface defects in different dimensions (1D, 2D, and 3D), including precious metal atoms, doping various atoms or ions, creating heterojunctions, and utilizing auxiliary catalysts. The significance of the active site in the photocatalytic nitrogen fixation mechanism lies in its ability to adsorb and activate N₂ molecules, while also facilitating the transmission of photogenerated electrons to the adsorbed nitrogen molecules. The phenomenon being investigated is primarily observed in materials with a high surface area, such as one-dimensional nanomaterials. The inclusion of oxygen vacancies enhances the light absorption spectrum of numerous photocatalysts that rely on oxygen vacancies as active sites. Nevertheless, it is crucial to recognize that an excessive prevalence of oxygen vacancies is considered detrimental. The presence of an excessive quantity of oxygen vacancies can hinder the nitrogen reduction process by providing sites for the recombination of electron–hole pairs. One approach to enhancing catalytic nitrogen fixation involves deliberately increasing the number of nitrogen vacancies. In recent years, there has been a significant surge in the popularity of photocatalytic nitrogen fixation catalysts featuring one-dimensional nanomaterials with a substantial number of active sites. The activation of the N₂ molecule, the weakening of the N≡N triple bond, and the promotion of N₂ reduction to NH₃ can be facilitated through electronic feedback mechanisms. In addition to the aforementioned achievements, significant efforts must be made to enhance both the quantity and efficacy of active sites on the catalyst’s surface. This is crucial for increasing the photocatalyst’s ability to effectively convert nitrogen under solar irradiation. Consequently, thorough research and investigation into multiple issues are imperative.

In future nitrogen fixation investigations, it is conceivable to integrate various active sites to explore nitrogen fixation, such as investigating nitrogen fixation in the context of nitrogen vacancies and oxygen vacancies. Furthermore, nitrogen exhibits low solubility in aqueous solutions. Therefore, it may be worthwhile to explore potential improvements to the current aqueous photocatalytic nitrogen fixation reaction system. These enhancements could include examining the catalyst-to-water ratio, incorporating ionic liquids, exploring

the gas–solid system, and investigating the utilization of heat for light conversion instead of relying solely on cooling water. Moreover, in subsequent research, active site computation and in situ experimentation could be employed to evaluate the catalytic reaction mechanism, and a suitable catalyst could be developed based on the computational findings.

Author Contributions: Conceptualization, V.B.K. and R.N.R.; methodology, V.B.K.; validation, V.B.K. and R.N.R. formal analysis, S.P.D. and S.J.K.; investigation, V.B.K.; resources, original draft preparation, V.B.K. and R.N.R.; writing—review and editing, S.P.D. and S.J.K.; visualization V.B.K. supervision, and project administration. All authors have read and agreed to the published version of the manuscript.

Funding: This research received no external funding.

Data Availability Statement: All the necessary data is added in present article.

Acknowledgments: The authors would like to thank the Ministry of Science and Technology Taiwan and Shivaji University Kolhapur (MS) India.

Conflicts of Interest: The authors declare no conflict of interest.

References

1. Huang, R.; Li, X.; Gao, W.; Zhang, X.; Liang, S.; Luo, M. Recent advances in photocatalytic nitrogen fixation: From active sites to ammonia quantification methods. *RSC Adv.* **2021**, *11*, 14844–14861. [[CrossRef](#)] [[PubMed](#)]
2. Ghaly, A.; Ramakrishnan, V. Nitrogen sources and cycling in the ecosystem and its role in air, water and soil pollution: A critical review. *J. Pollut. Eff. Control* **2015**, *3*, 1000136.
3. Chen, X.; Li, N.; Kong, Z.; Ong, W.-J.; Zhao, X. Photocatalytic fixation of nitrogen to ammonia: State-of-the-art advancements and future prospects. *Mater. Horiz.* **2018**, *5*, 9–27. [[CrossRef](#)]
4. Wang, W.; Ji, Z.; Zhang, D.; Sun, P.; Duan, J. TiO₂ doped HKUST-1/CM film in the three-phase photocatalytic ammonia synthesis system. *Ceram. Int.* **2021**, *47*, 19180–19190. [[CrossRef](#)]
5. Wu, R.; Yi, J.; Bao, R.; Liu, P. The excellent photocatalytic capability of TiO₂@C/O-doped g-C₃N₄ heterojunction photocatalyst. *Colloids Surf. A* **2022**, *648*, 129351. [[CrossRef](#)]
6. Zhao, Y.; Zhou, S.; Zhao, J.; Du, Y.; Dou, S. Control of photocarrier separation and recombination at bismuth oxyhalide interface for nitrogen fixation. *J. Phys. Chem. Lett.* **2020**, *11*, 9304–9312. [[CrossRef](#)] [[PubMed](#)]
7. Deshmukh, S.; Pawar, K.; Koli, V.; Pachfule, P. Emerging graphitic carbon nitride-based nanobiomaterials for biological applications. *ACS Appl. Bio Mater.* **2023**, *6*, 1339–1367. [[CrossRef](#)] [[PubMed](#)]
8. Wang, J.; Zhao, C.; Yuan, S.; Li, X.; Zhang, J.; Hu, X.; Lin, H.; Wu, Y.; He, Y. One-step fabrication of Cu-doped Bi₂MoO₆ microflower for enhancing performance in photocatalytic nitrogen fixation. *J. Colloid Interface Sci.* **2023**, *638*, 427–438. [[CrossRef](#)] [[PubMed](#)]
9. Yu, X.; Qiu, H.; Wang, Z.; Wang, B.; Meng, Q.; Sun, S.; Tang, Y.; Zhao, K. Constructing the Z-scheme TiO₂/Au/BiOI nanocomposite for enhanced photocatalytic nitrogen fixation. *Appl. Surf. Sci.* **2021**, *556*, 149785. [[CrossRef](#)]
10. Xia, Y.; Yang, P.; Sun, Y.; Wu, Y.; Mayers, B.; Gates, B.; Yin, Y.; Kim, F.; Yan, H. One-dimensional nanostructures: Synthesis, characterization, and applications. *Adv. Mater.* **2003**, *15*, 353–389. [[CrossRef](#)]
11. Zhang, L.; Hou, S.; Wang, T.; Liu, S.; Gao, X.; Wang, C.; Wang, G. Recent advances in application of graphitic carbon nitride-based catalysts for photocatalytic nitrogen fixation. *Small* **2022**, *18*, 2202252. [[CrossRef](#)] [[PubMed](#)]
12. Comer, B.; Nazemi, M.; Hatzell, M.; Medford, A. Analysis of Photocatalytic Nitrogen Fixation on Rutile TiO₂ (110). *ACS Sustain. Chem. Eng.* **2017**, *6*, 4648–4660. [[CrossRef](#)]
13. Yang, J.; Huang, Z.; Meng, Y.; Ni, Z.; Xie, B.; Xia, S. Experimental and theoretical study on photocatalytic nitrogen reduction catalyzed by Fe doped MoO₂. *Sep. Purif. Technol.* **2023**, *318*, 124019. [[CrossRef](#)]
14. Xu, T.; Liang, J.; Li, S.; Xu, Z.; Yue, L.; Li, T.; Luo, Y.; Liu, Q.; Shi, X.; Asiri, A.M.; et al. Recent Advances in Nonprecious Metal Oxide Electrocatalysts and Photocatalysts for N₂ Reduction Reaction under Ambient Condition. *Small Sci.* **2021**, *1*, 2000069. [[CrossRef](#)]
15. Hirakawa, H.; Hashimoto, M.; Shiraishi, Y.; Hirai, T. Photocatalytic Conversion of Nitrogen to Ammonia with Water on Surface Oxygen Vacancies of Titanium Dioxide. *J. Am. Chem. Soc.* **2017**, *139*, 10929–10936. [[CrossRef](#)] [[PubMed](#)]
16. Wang, S.; Hai, X.; Ding, X.; Chang, K.; Xiang, Y.; Meng, X.; Yang, Z.; Chen, H.; Ye, J. Light-switchable oxygen vacancies in ultrafine Bi₅O₇Br nanotubes for boosting solar-driven nitrogen fixation in pure water. *Adv. Mater.* **2017**, *29*, 1701774. [[CrossRef](#)] [[PubMed](#)]
17. Zhang, N.; Jalil, A.; Wu, D.; Chen, S.; Liu, Y.; Gao, C.; Ye, W.; Qi, Z.; Ju, H.; Wang, C. Refining defect states in W₁₈O₄₉ by Mo doping: A strategy for tuning N₂ activation towards solar-driven nitrogen fixation. *J. Am. Chem. Soc.* **2018**, *140*, 9434–9443. [[CrossRef](#)] [[PubMed](#)]
18. Mousavi, M.; Habibi, M.M.; Zhang, G.; Moradian, S.; Ghasemi, J.B. In-situ construction of ZnO/Sb₂MoO₆ heterostructure for efficient visible-light photocatalytic N₂ fixation to NH₃. *J. Am. Chem. Soc.* **2018**, *140*, 9434–9443.

19. Dolla, T.H.; Mathews, T.; Maxakato, N.W.; Ndungu, P.; Montini, T. Recent advances in transition metal sulfide-based electrocatalysts and photocatalysts for nitrogen fixation. *J. Electroanal. Chem.* **2022**, *928*, 117049. [[CrossRef](#)]
20. Hao, Q.; Liu, C.; Jia, G.; Wang, Y.; Arandiyana, H.; Wei, W.; Ni, B. Catalytic reduction of nitrogen to produce ammonia by bismuth-based catalysts: State of the art and future prospects. *Mater. Horiz.* **2020**, *7*, 1014–1029. [[CrossRef](#)]
21. Huang, Y.; Zhang, N.; Wu, Z.; Xie, X. Artificial nitrogen fixation over bismuth-based photocatalysts: Fundamentals and future perspectives. *J. Mater. Chem. A* **2020**, *8*, 4978–4995. [[CrossRef](#)]
22. Guo, W.; Zhang, K.; Liang, Z.; Zou, R.; Xu, Q. Electrochemical nitrogen fixation and utilization: Theories, advanced catalyst materials and system design. *Chem. Soc. Rev.* **2019**, *48*, 5658–5716. [[CrossRef](#)] [[PubMed](#)]
23. Li, X.F.; Li, Q.K.; Cheng, J.; Liu, L.; Yan, Q.; Wu, Y.; Zhang, X.H.; Wang, Z.Y.; Qiu, Q.; Luo, Y. Conversion of dinitrogen to ammonia by FeN₃-embedded graphene. *J. Am. Chem. Soc.* **2016**, *138*, 8706–8709. [[CrossRef](#)] [[PubMed](#)]
24. Hao, D.; Liu, Y.; Gao, S.; Arandiyana, H.; Bai, X.; Kong, Q.; Wei, W.; Shen, P.K.; Ni, B. Emerging artificial nitrogen cycle processes through novel electrochemical and photochemical synthesis. *Mater. Today* **2021**, *46*, 212–233. [[CrossRef](#)]
25. Ling, C.; Zhang, Y.; Li, Q.; Bai, X.; Shi, L.; Wang, J. New mechanism for N₂ reduction: The Essential Role of Surface Hydrogenation. *J. Am. Chem. Soc.* **2019**, *141*, 18264–18270. [[CrossRef](#)]
26. Azofra, L.M.; Li, N.; MacFarlane, D.R.; Sun, C. Promising prospects for 2D d 2-d 4 M 3 C 2 transition metal carbides (MXenes) in N₂ capture and conversion into ammonia. *Energy Environ. Sci.* **2016**, *9*, 2545–2549. [[CrossRef](#)]
27. Cheng, M.; Xiao, C.; Xie, Y. Photocatalytic nitrogen fixation: The role of defects in photocatalysts. *J. Mater. Chem. A* **2019**, *7*, 19616–19633. [[CrossRef](#)]
28. Wagner, R.S.; Ellis, W.C. Vapor-liquid-solid mechanism of single crystal growth. *Appl. Phys. Lett.* **1964**, *4*, 89–90. [[CrossRef](#)]
29. Garnett, E.; Mai, L.; Yang, P. Introduction: 1D nanomaterials/nanowires. *Chem. Rev.* **2019**, *119*, 8955–8957. [[CrossRef](#)] [[PubMed](#)]
30. Tersoff, J.; Ruoff, R.S. Structural properties of a carbon-nanotube crystal. *Phys. Rev. Lett.* **1994**, *73*, 676–679. [[CrossRef](#)] [[PubMed](#)]
31. Yamabe, T. Recent development of carbon nanotube. *Synth. Met.* **1995**, *70*, 1511–1518. [[CrossRef](#)]
32. Qin, L.-C.; Zhao, X.; Hirahara, K.; Miyamoto, Y.; Ando, Y.; Iijima, S. The smallest carbon nanotube. *Nature* **2000**, *408*, 50. [[CrossRef](#)] [[PubMed](#)]
33. Hu, J.; Odom, T.W.; Lieber, C.M. Chemistry and Physics in One Dimension: Synthesis and Properties of Nanowires and Nanotubes. *Acc. Chem. Res.* **1999**, *32*, 435–445. [[CrossRef](#)]
34. Zhang, Y.; Dai, H. Formation of metal nanowires on suspended single-walled carbon nanotubes. *Appl. Phys. Lett.* **2000**, *77*, 3015–3017. [[CrossRef](#)]
35. Zhang, Y.F.; Tang, Y.H.; Wang, N.; Lee, C.S.; Bello, I.; Lee, S.T. One-dimensional growth mechanism of crystalline silicon nanowires. *J. Cryst. Growth* **1999**, *197*, 136–140. [[CrossRef](#)]
36. Duan, X.; Lieber, C.M. General synthesis of compound semiconductor nanowires. *Adv. Mater.* **2000**, *12*, 298–302. [[CrossRef](#)]
37. Sun, Y. Silver nanowires—Unique templates for functional nanostructures. *Nanoscale* **2010**, *2*, 1626–1642. [[CrossRef](#)] [[PubMed](#)]
38. Morales, A.M.; Lieber, C.M. A Laser Ablation Method for the Synthesis of Crystalline Semiconductor Nanowires. *Science* **1998**, *279*, 208–211. [[CrossRef](#)] [[PubMed](#)]
39. Zheng, F.-L.; Li, G.-R.; Ou, Y.-N.; Wang, Z.-L.; Su, C.-Y.; Tong, Y.-X. Synthesis of hierarchical rippled Bi₂O₃ nanobelts for supercapacitor applications. *Chem. Commun.* **2010**, *46*, 5021–5023. [[CrossRef](#)] [[PubMed](#)]
40. Dharmaraj, N.; Kim, C.H.; Kim, H.Y. Pb(Zr_{0.5}, Ti_{0.5})O₃ nanofibres by electrospinning. *Mater. Lett.* **2005**, *59*, 3085–3089. [[CrossRef](#)]
41. Rao, C.N.R.; Satishkumar, B.C.; Govindaraj, A.; Nath, M. Nanotubes. *ChemPhysChem* **2001**, *2*, 78–105. [[CrossRef](#)] [[PubMed](#)]
42. Xiao, F.-X.; Miao, J.; Tao, H.B.; Hung, S.-F.; Wang, H.-Y.; Yang, H.B.; Chen, J.; Chen, R.; Liu, B. One-Dimensional hybrid nanostructures for heterogeneous photocatalysis and photoelectrocatalysis. *Small* **2015**, *11*, 2115–2131. [[CrossRef](#)] [[PubMed](#)]
43. Weng, B.; Liu, S.; Tang, Z.-R.; Xu, Y.-J. One-dimensional nanostructure based materials for versatile photocatalytic applications. *RSC Adv.* **2014**, *4*, 12685–12700. [[CrossRef](#)]
44. Shang, H.; Chen, H.; Dai, M.; Hu, Y.; Gao, F.; Yang, H.; Xu, B.; Zhang, S.; Tan, B.; Zhang, X.; et al. A mixed-dimensional 1D Se–2D InSe van der Waals heterojunction for high responsivity self-powered photodetectors. *Nanoscale Horiz.* **2020**, *5*, 564–572. [[CrossRef](#)] [[PubMed](#)]
45. Cheong, J.Y.; Cho, S.-H.; Lee, J.; Jung, J.-W.; Kim, C.; Kim, I.-D. Multifunctional 1D Nanostructures toward Future Batteries: A Comprehensive Review. *Adv. Funct. Mater.* **2022**, *32*, 2208374. [[CrossRef](#)]
46. Zhong, Y.; Peng, C.; He, Z.; Chen, D.; Jia, H.; Zhang, J.; Ding, H.; Wu, X. Interface engineering of heterojunction photocatalysts based on 1D nanomaterials. *Catal. Sci. Technol.* **2021**, *11*, 27–42. [[CrossRef](#)]
47. Li, L.; Zhao, C.; Zhang, L.; Zhu, Y. γ -GeSe nanotubes: A one-dimensional semiconductor with high carrier mobility potential for photocatalytic water splitting. *J. Mater. Chem. C* **2021**, *9*, 15158–15164. [[CrossRef](#)]
48. Wang, L.; Wu, W.; Liang, K.; Yu, X. Advanced strategies for improving the photocatalytic nitrogen fixation performance: A short review. *Energy Fuels* **2022**, *36*, 11278–11291. [[CrossRef](#)]
49. Wang, Z.; Huang, Y.; Chen, M.; Shi, X.; Zhang, Y.; Cao, J.; Ho, W.; Lee, S.C. Roles of N-vacancies over porous g-C₃N₄ microtubes during photocatalytic NO_x removal. *ACS Appl. Mater. Interfaces* **2019**, *11*, 10651–10662. [[CrossRef](#)] [[PubMed](#)]
50. Li, X.; Shi, H.; Yan, X.; Zuo, S.; Zhang, Y.; Wang, T.; Luo, S.; Yao, C.; Ni, C. Palygorskite immobilized direct Z-scheme nitrogen-doped carbon quantum dots/PrFeO₃ for Photo-SCR Removal of NO_x. *ACS Sustain. Chem. Eng.* **2018**, *6*, 10616–10627. [[CrossRef](#)]
51. Mirzaei, A.; Chen, Z.; Haghighat, F.; Yerushalmi, L. Removal of pharmaceuticals and endocrine disrupting compounds from water by zinc oxide-based photocatalytic degradation: A review. *Sustain. Cities Soc.* **2016**, *27*, 407–418. [[CrossRef](#)]

52. Li, M.; Zhang, L.; Fan, X.; Wu, M.; Wang, M.; Cheng, R.; Zhang, L.; Yao, H.; Shi, J. Core-shell LaPO₄/g-C₃N₄ nanowires for highly active and selective CO₂ reduction. *Appl. Catal. B* **2017**, *201*, 629–635. [CrossRef]
53. Lu, Y.; Zhang, J.; Ge, L.; Han, C.; Qiu, P.; Fang, S. Synthesis of novel AuPd nanoparticles decorated one-dimensional ZnO nanorod arrays with enhanced photoelectrochemical water splitting activity. *J. Colloid Interface Sci.* **2016**, *483*, 146–153. [CrossRef] [PubMed]
54. Mei, F.; Dai, K.; Zhang, J.; Li, W.; Liang, C. Construction of Ag SPR-promoted step-scheme porous g-C₃N₄/Ag₃VO₄ heterojunction for improving photocatalytic activity. *Appl. Surf. Sci.* **2019**, *488*, 151–160. [CrossRef]
55. Wang, J.; Lin, W.; Ran, Y.; Cui, J.; Wang, L.; Yu, X.; Zhang, Y. Nanotubular TiO₂ with Remedied defects for photocatalytic nitrogen fixation. *J. Phys. Chem. C* **2020**, *124*, 1253–1259. [CrossRef]
56. Li, C.; Gu, M.; Gao, M.; Liu, K.; Zhao, X.; Cao, N.; Feng, J.; Ren, Y.; Wei, T.; Zhang, M. N-doping TiO₂ hollow microspheres with abundant oxygen vacancies for highly photocatalytic nitrogen fixation. *J. Colloid Interface Sci.* **2022**, *609*, 341–352. [CrossRef] [PubMed]
57. Hao, C.; Liao, Y.; Wu, Y.; An, Y.; Lin, J.; Gu, Z.; Jiang, M.; Hu, S.; Wang, X. RuO₂-loaded TiO₂-MXene as a high performance photocatalyst for nitrogen fixation. *J. Phys. Chem. Solids* **2020**, *136*, 109141. [CrossRef]
58. Yin, S.; Liu, S.; Zhang, H.; Jiao, S.; Xu, Y.; Wang, Z.; Li, X.; Wang, L.; Wang, H. Engineering one-Dimensional AuPd Nanospikes for Efficient Electrocatalytic Nitrogen Fixation. *ACS Appl. Mater. Interfaces* **2021**, *13*, 20233–20239. [CrossRef] [PubMed]
59. Wang, J.; Yu, L.; Hu, L.; Chen, G.; Xin, H.; Feng, X. Ambient ammonia synthesis via palladium-catalyzed electrohydrogenation of dinitrogen at low overpotential. *Nat. Commun.* **2018**, *9*, 1795. [CrossRef] [PubMed]
60. Wang, J.; Huang, B.; Ji, Y.; Sun, M.; Wu, T.; Yin, R.; Zhu, X.; Li, Y.; Shao, Q.; Huang, X. A general strategy to glassy M-Te (M = Ru, Rh, Ir) porous nanorods for efficient electrochemical N₂ fixation. *Adv. Mater.* **2020**, *32*, 1907112. [CrossRef]
61. Jiao, X.; Chen, Z.; Li, X.; Sun, Y.; Gao, S.; Yan, W.; Wang, C.; Zhang, Q.; Lin, Y.; Luo, Y. Defect-mediated electron-hole separation in one-unit-cell ZnIn₂S₄ layers for boosted solar-driven CO₂ reduction. *J. Am. Chem. Soc.* **2017**, *139*, 7586–7594. [CrossRef] [PubMed]
62. Gao, S.; Gu, B.; Jiao, X.; Sun, Y.; Zu, X.; Yang, F.; Zhu, W.; Wang, C.; Feng, Z.; Ye, B.; et al. Highly efficient and exceptionally durable CO₂ photoreduction to methanol over freestanding defective single-unit-cell bismuth vanadate layers. *J. Am. Chem. Soc.* **2017**, *139*, 3438–3445. [CrossRef] [PubMed]
63. Hu, L.; Yang, H.; Wang, S.; Gao, J.; Hou, H.; Yang, W. MOF-derived hexagonal In₂O₃ microrods decorated with g-C₃N₄ ultrathin nanosheets for efficient photocatalytic hydrogen production. *J. Mater. Chem. C* **2021**, *9*, 5343–5348. [CrossRef]
64. Bariki, R.; Das, K.; Pradhan, S.K.; Prusti, B.; Mishra, B. MOF-derived hollow tubular In₂O₃/MIIIn₂S₄ (MII: Ca, Mn, and Zn) heterostructures: Synergetic charge-transfer mechanism and excellent photocatalytic performance to boost activation of small atmospheric molecules. *ACS Appl. Energy Mater.* **2022**, *5*, 11002–11017. [CrossRef]
65. Dong, G.; Huang, X.; Bi, Y. Anchoring Black Phosphorus Quantum Dots on Fe-Doped W₁₈O₄₉ Nanowires for Efficient Photocatalytic Nitrogen Fixation. *Angew. Chem.* **2022**, *134*, e202204271. [CrossRef]
66. Yang, J.; Ruan, Z.; Jiang, S.; Xia, P.; Yang, Q.; Zhang, Q.; Xiao, C.; Xie, Y. Ce-doped W₁₈O₄₉ nanowires for tuning N₂ activation toward direct nitrate photosynthesis. *J. Phys. Chem. Lett.* **2021**, *12*, 11295–11302. [CrossRef]
67. Li, Y.; Qian, F.; Xiang, J.; Lieber, C. Nanowire electronic and optoelectronic devices. *Mater. Today* **2006**, *9*, 18–27. [CrossRef]
68. Helveg, S.; López-Cartes, C.; Sehested, J.; Hansen, P.L.; Clausen, B.S.; Rostrup-Nielsen, J.R.; Abild-Pedersen, F.; Nørskov, J. Atomic-scale imaging of carbon nanofibre growth. *Nature* **2004**, *427*, 426–429. [CrossRef] [PubMed]
69. Meister, S.; Peng, H.; McIlwrath, K.; Jarausch, K.; Zhang, X.F.; Cui, Y. Synthesis and characterization of phase-change nanowires. *Nano Lett.* **2006**, *6*, 1514–1517. [CrossRef] [PubMed]
70. Yang, P.; Lieber, C. Nanorod-superconductor composites: A pathway to materials with high critical current densities. *Science* **1996**, *273*, 1836–1840. [CrossRef]
71. Park, W.I.; Kim, D.H.; Jung, S.-W.; Yi, G.-C. Metalorganic vapor-phase epitaxial growth of vertically well-aligned ZnO nanorods. *Appl. Phys. Lett.* **2002**, *80*, 4232–4234. [CrossRef]
72. Liu, Z.; Zhang, D.; Han, S.; Li, C.; Tang, T.; Jin, W.; Liu, X.; Lei, B.; Zhou, C. Laser ablation synthesis and electron transport studies of tin oxide nanowires. *Adv. Mater.* **2003**, *15*, 1754–1757. [CrossRef]
73. Udom, I.; Ram, M.K.; Stefanakos, E.K.; Hepp, A.F.; Goswami, D.Y. One dimensional-ZnO nanostructures: Synthesis, properties and environmental applications. *Mater. Sci. Semicond. Process.* **2013**, *16*, 2070–2083. [CrossRef]
74. Miao, J.; Liu, B. II–VI semiconductor nanowires: ZnO. In *Semiconductor Nanowires*; Elsevier: Amsterdam, The Netherlands, 2015; pp. 3–28.
75. Kislyuk, V.; Dimitriev, O. Nanorods and nanotubes for solar cells. *J. Nanosci. Nanotechnol.* **2008**, *8*, 131–148. [CrossRef] [PubMed]
76. Anastasescu, C.; Mihaiu, S.; Preda, S.; Zaharescu, M. *1D Oxide Nanostructures Obtained by Sol-Gel and Hydrothermal Methods*; Springer: Berlin/Heidelberg, Germany, 2016.
77. Zargari, S.; Yaghoubi Berijani, M.; Rahimi, R. Synthesis of ZnO nanorods via coprecipitation method and its sensitizing with tetrakis (4-carboxy phenyl) porphyrin and its tin complex to enhance the visible light photocatalytic activity. *J. Nanomater.* **2014**, *4*, 161.
78. Soares, A.S.; Araujo, F.P.; Osajima, J.A.; Guerra, Y.; Viana, B.C.; Peña-Garcia, R. Nanotubes/nanorods-like structures of La-doped ZnO for degradation of Methylene Blue and Ciprofloxacin. *J. Photochem. Photobiol. A* **2024**, *447*, 115235. [CrossRef]
79. Wang, F.; Yang, H.; Zhang, H.; Jiang, J. Growth process and enhanced photocatalytic performance of CuBi₂O₄ hierarchical microcuboids decorated with AuAg alloy nanoparticles. *J. Mater. Sci. Mater. Electron.* **2018**, *29*, 1304–1316. [CrossRef]

80. Koli, V.B.; Murugan, G.; Ke, S.-C. Self-assembled synthesis of porous iron-doped graphitic carbon nitride nanostructures for efficient photocatalytic hydrogen evolution and nitrogen fixation. *Nanomaterials* **2023**, *13*, 275. [[CrossRef](#)] [[PubMed](#)]
81. Chen, F.; Zhu, Y.-J.; Wang, K.-W.; Zhao, K.-L. Surfactant-free solvothermal synthesis of hydroxyapatite nanowire/nanotube ordered arrays with biomimetic structures. *CrystEngComm* **2011**, *13*, 1858–1863. [[CrossRef](#)]
82. Zeng, Y.; Zhang, W.; Xu, C.; Xiao, N.; Huang, Y.; Yu, D.Y.W.; Hng, H.H.; Yan, Q. One-step solvothermal synthesis of single-crystalline TiOF₂ nanotubes with high lithium-ion battery performance. *Chem. Eur. J.* **2012**, *18*, 4026–4030. [[CrossRef](#)] [[PubMed](#)]
83. Alkanad, K.; Hezam, A.; Al-Zaqri, N.; Bajiri, M.A.; Alnaggar, G.; Drmosh, Q.A.; Almukhlifi, H.A.; Neratur Krishnappagowda, L. One-Step Hydrothermal Synthesis of Anatase TiO₂ Nanotubes for Efficient Photocatalytic CO₂ Reduction. *ACS Omega* **2022**, *7*, 38686–38699. [[CrossRef](#)] [[PubMed](#)]
84. Yong, S.-M.; Muralidharan, P.; Jo, S.H.; Kim, D.K. One-step hydrothermal synthesis of CdTe nanowires with amorphous carbon sheaths. *Mater. Lett.* **2010**, *64*, 1551–1554. [[CrossRef](#)]
85. Vijayakumar; Shivaraj, B.W.; Manjunatha, C.; Abhishek, B.; Nagaraju, G.; Panda, P.K. Hydrothermal synthesis of ZnO nanotubes for CO gas sensing. *Sens. Int.* **2020**, *1*, 100018. [[CrossRef](#)]
86. Ge, M.; Li, Q.; Cao, C.; Huang, J.; Li, S.; Zhang, S.; Chen, Z.; Zhang, K.; Al-Deyab, S.S.; Lai, Y.J. One-dimensional TiO₂ nanotube photocatalysts for solar water splitting. *Adv. Sci.* **2017**, *4*, 1600152. [[CrossRef](#)] [[PubMed](#)]
87. Wang, Y.; Wang, Q.; Zhan, X.; Wang, F.; Safdar, M.; He, J. Visible light driven type II heterostructures and their enhanced photocatalysis properties: A review. *Nanoscale* **2013**, *5*, 8326–8339. [[CrossRef](#)] [[PubMed](#)]
88. Wang, C.; Ying, J. Sol–gel synthesis and hydrothermal processing of anatase and rutile titania nanocrystals. *Chem. Mater.* **1999**, *11*, 3113–3120. [[CrossRef](#)]
89. Kaur, A.; Bajaj, B.; Kaushik, A.; Saini, A.; Sud, D. A review on template assisted synthesis of multi-functional metal oxide nanostructures: Status and prospects. *Mater. Sci. Eng. B* **2022**, *286*, 116005. [[CrossRef](#)]
90. Sadeghzadeh Attar, A.; Sasani Ghamsari, M.; Hajiesmaeilbaigi, F.; Mirdamadi, S.; Katagiri, K.; Koumoto, K. Synthesis and characterization of anatase and rutile TiO₂ nanorods by template-assisted method. *J. Mater. Sci.* **2008**, *43*, 5924–5929. [[CrossRef](#)]
91. Pashchanka, M.; Engstler, J.; Schneider, J.J.; Siozios, V.; Fasel, C.; Hauser, R.; Kinski, I.; Riedel, R.; Lauterbach, S.; Kleebe, H.J. Polymer-derived sioc nanotubes and nanorods via a template approach. *Eur. J. Inorg. Chem.* **2009**, *23*, 3496–3506. [[CrossRef](#)]
92. Bhattarai, D.P.; Hwang, T.I.; Kim, J.I.; Lee, J.H.; Chun, S.; Kim, B.-S.; Park, C.H.; Kim, C. Synthesis of polypyrrole nanorods via sacrificial removal of aluminum oxide nanopore template: A study on cell viability, electrical stimulation and neuronal differentiation of PC12 cells. *Mater. Sci. Eng. C* **2020**, *107*, 110325. [[CrossRef](#)] [[PubMed](#)]
93. Caruso, F.; Caruso, R.A.; Mohwald, H. Nanoengineering of inorganic and hybrid hollow spheres by colloidal templating. *Science* **1998**, *282*, 1111–1114. [[CrossRef](#)] [[PubMed](#)]
94. Yong, K.-T.; Sahoo, Y.; Swihart, M.T.; Prasad, P. Synthesis and plasmonic properties of silver and gold nanoshells on polystyrene cores of different size and of gold–silver core–shell nanostructures. *Colloids Surf. A* **2006**, *290*, 89–105. [[CrossRef](#)]
95. Poolakkandy, R.R.; Menampambath, M. Soft-template-assisted synthesis: A promising approach for the fabrication of transition metal oxides. *Nanoscale Adv.* **2020**, *2*, 5015–5045. [[CrossRef](#)] [[PubMed](#)]
96. Tiano, A.L.; Koenigsmann, C.; Santulli, A.C.; Wong, S. Solution-based synthetic strategies for one-dimensional metal-containing nanostructures. *Chem. Commun.* **2010**, *46*, 8093–8130. [[CrossRef](#)] [[PubMed](#)]
97. Chen, Y.; Liu, Y.; Lu, S.; Xu, C.; Shao, C.; Wang, C.; Zhang, J.; Lu, Y.; Shen, D.; Fan, X. Optical properties of ZnO and ZnO: In nanorods assembled by sol-gel method. *J. Chem. Phys.* **2005**, *123*, 134701. [[CrossRef](#)] [[PubMed](#)]
98. Wang, X.; Wang, X.; Huang, W.; Sebastian, P.; Gamboa, S. Sol–gel template synthesis of highly ordered MnO₂ nanowire arrays. *J. Power Sources* **2005**, *140*, 211–215. [[CrossRef](#)]
99. Matysiak, W.; Tański, T.; Smok, W.; Polishchuk, O. Synthesis of hybrid amorphous/crystalline SnO₂ 1D nanostructures: Investigation of morphology, structure and optical properties. *Sci. Rep.* **2020**, *10*, 14802. [[CrossRef](#)] [[PubMed](#)]
100. Rodríguez-Reyes, M.; Dorantes-Rosales, H. A simple route to obtain TiO₂ nanowires by the sol–gel method. *J. Sol-Gel Sci. Technol.* **2011**, *59*, 658–661. [[CrossRef](#)]
101. Whitney, T.; Searson, P.; Jiang, J.; Chien, C. Fabrication and magnetic properties of arrays of metallic nanowires. *Science* **1993**, *261*, 1316–1319. [[CrossRef](#)] [[PubMed](#)]
102. She, G.; Mu, L.; Shi, W. Electrodeposition of One-dimensional nanostructures. *Recent Pat. Nanotechnol.* **2009**, *3*, 182–191. [[CrossRef](#)]
103. Ge, M.; Cao, C.; Huang, J.; Li, S.; Chen, Z.; Zhang, K.-Q.; Al-Deyab, S.; Lai, Y. A review of one-dimensional TiO₂ nanostructured materials for environmental and energy applications. *J. Mater. Chem. A* **2016**, *4*, 6772–6801. [[CrossRef](#)]
104. Györi, Z.; Kónya, Z.; Kukovecz, Á. Visible light activation photocatalytic performance of PbSe quantum dot sensitized TiO₂ Nanowires. *Appl. Catal.* **2015**, *179*, 583–588. [[CrossRef](#)]
105. Ahn, S.H.; Chi, W.S.; Park, J.T.; Koh, J.K.; Roh, D.K.; Kim, J.H. Direct assembly of preformed nanoparticles and graft copolymer for the fabrication of micrometer-thick, organized TiO₂ films: High efficiency solid-state dye-sensitized solar cells. *Adv. Mater.* **2012**, *24*, 519–522. [[CrossRef](#)] [[PubMed](#)]
106. Wu, S.; Tan, X.; Liu, K.; Lei, J.; Wang, L.; Zhang, J. TiO₂ (B) nanotubes with ultrathin shell for highly efficient photocatalytic fixation of nitrogen. *Catal. Today* **2019**, *335*, 214–220. [[CrossRef](#)]
107. Chang, S.; Xu, X. Au nanocrystals decorated TiO₂ nanotubes for photocatalytic nitrogen fixation into ammonia. *Inorg. Chem. Front.* **2020**, *7*, 620–624. [[CrossRef](#)]

108. Huang, M.H.; Wu, Y.; Feick, H.; Tran, N.; Weber, E.; Yang, P. Catalytic Growth of Zinc Oxide Nanowires by Vapor Transport. *Adv. Mater.* **2001**, *13*, 113–116. [[CrossRef](#)]
109. Pan, Z.W.; Dai, Z.R.; Wang, Z.L. Nanobelts of Semiconducting Oxides. *Science* **2001**, *291*, 1947–1949. [[CrossRef](#)] [[PubMed](#)]
110. Ray, A.; Sultana, S.; Tripathy, S.P.; Parida, K. Aggrandizing the Photoactivity of ZnO Nanorods toward N₂ Reduction and H₂ Evolution through Facile In Situ Coupling with Ni₃Py. *ACS Sustain. Chem. Eng.* **2021**, *9*, 6305–6317. [[CrossRef](#)]
111. Wang, L.; Li, M.; Zhang, Q.; Li, F.; Xu, L. Constructing electron transfer pathways and active centers over W₁₈O₄₉ nanowires by doping Fe³⁺ and incorporating g-C₃N₅ for enhanced photocatalytic nitrogen fixation. *Inorg. Chem. Front.* **2021**, *8*, 3566–3575. [[CrossRef](#)]
112. Vu, M.-H.; Nguyen, C.-C.; Do, T.-O. Synergistic Effect of Fe Doping and Plasmonic Au Nanoparticles on W₁₈O₄₉ Nanorods for Enhancing Photoelectrochemical Nitrogen Reduction. *ACS Sustain. Chem. Eng.* **2020**, *8*, 12321–12330. [[CrossRef](#)] [[PubMed](#)]
113. Hui, X.; Li, L.; Xia, Q.; Hong, S.; Hao, L.; Robertson, A.W.; Sun, Z. Interface engineered Sb₂O₃/W₁₈O₄₉ heterostructure for enhanced visible-light-driven photocatalytic N₂ reduction. *Chem. Eng. J.* **2022**, *438*, 135485. [[CrossRef](#)]
114. Shang, H.; Wang, Y.; Jia, H.; Qu, M.; Ye, X.; Zhu, Q.; Zhang, D.; Wang, D.; Li, G.; Li, H. Constructing asymmetric active sites on defective Ru/W₁₈O₄₉ for photocatalytic nitrogen fixation. *Catal. Sci. Technol.* **2023**, *13*, 854–861. [[CrossRef](#)]
115. Xing, P.; Chen, P.; Chen, Z.; Hu, X.; Lin, H.; Wu, Y.; Zhao, L.; He, Y. Novel Ternary MoS₂/C-ZnO Composite with efficient performance in photocatalytic NH₃ synthesis under simulated sunlight. *ACS Sustain. Chem. Eng.* **2018**, *6*, 14866–14879. [[CrossRef](#)]
116. Li, X.; Wang, W.; Jiang, D.; Sun, S.; Zhang, L.; Sun, X. Efficient Solar-Driven Nitrogen Fixation over Carbon–Tungstic-Acid Hybrids. *Chem. Eur. J.* **2016**, *22*, 13819–13822. [[CrossRef](#)] [[PubMed](#)]
117. Zhu, Y.; Zheng, X.; Zhang, W.; Kheradmand, A.; Gu, S.; Kobielski, M.; Macyk, W.; Li, H.; Huang, J.; Jiang, Y. Near-Infrared-Triggered Nitrogen Fixation over Upconversion Nanoparticles Assembled Carbon Nitride Nanotubes with Nitrogen Vacancies. *ACS Appl. Mater. Interfaces* **2021**, *13*, 32937–32947. [[CrossRef](#)] [[PubMed](#)]
118. Wang, D.; Zhou, W.; Zhang, R.; Zeng, J.; Du, Y.; Qi, S.; Cong, C.; Ding, C.; Huang, X.; Wen, G. Mass production of large-sized, nonlayered 2D nanosheets: Their directed synthesis by a rapid “gel-blowing” strategy, and applications in Li/Na storage and catalysis. *Adv. Mater.* **2018**, *30*, 1803569. [[CrossRef](#)] [[PubMed](#)]
119. Li, Y.; Gu, M.; Shi, T.; Cui, W.; Zhang, X.; Dong, F.; Cheng, J.; Fan, J.; Lv, K. Carbon vacancy in C₃N₄ nanotube: Electronic structure, photocatalysis mechanism and highly enhanced activity. *Appl. Catal. B* **2020**, *262*, 118281. [[CrossRef](#)]
120. Zeng, Y.; Liu, X.; Liu, C.; Wang, L.; Xia, Y.; Zhang, S.; Luo, S.; Pei, Y. Scalable one-step production of porous oxygen-doped g-C₃N₄ nanorods with effective electron separation for excellent visible-light photocatalytic activity. *Appl. Catal. B* **2018**, *224*, 1–9. [[CrossRef](#)]
121. Zhang, D.; He, W.; Ye, J.; Gao, X.; Wang, D.; Song, J. Polymeric carbon nitride-derived photocatalysts for water splitting and nitrogen fixation. *Small* **2021**, *17*, 2005149. [[CrossRef](#)] [[PubMed](#)]
122. Hua, C.; Dong, X.; Zheng, N.; Zhang, X.; Xue, M. In situ fabrication of self-assembled BiOBr_xI_{1-x} coated on carbon nanofibers for efficient solar light-driven photocatalytic nitrogen fixation. *Sustain. Energy Fuels* **2020**, *4*, 6196–6202. [[CrossRef](#)]
123. He, Z.; Wang, Y.; Dong, X.; Zheng, N.; Ma, H.; Zhang, X. Indium sulfide nanotubes with sulfur vacancies as an efficient photocatalyst for nitrogen fixation. *RSC Adv.* **2019**, *9*, 21646–21652. [[CrossRef](#)]
124. Jia, L.; Tan, X.; Yu, T.; Ye, J. Mixed Metal Sulfides for the Application of Photocatalytic Energy Conversion. *Energy Fuels* **2022**, *36*, 11308–11322. [[CrossRef](#)]
125. Jamal, F.; Rafique, A.; Moeen, S.; Haider, J.; Nabgan, W.; Haider, A.; Imran, M.; Nazir, G.; Alhassan, M.; Ikram, M.; et al. Review of Metal Sulfide Nanostructures and their Applications. *ACS Appl. Nano Mater.* **2023**, *6*, 7077–7106. [[CrossRef](#)]
126. Chen, S.; Zhao, X.; Xie, F.; Tang, Z.; Wang, X. Efficient charge separation between ZnIn₂S₄ nanoparticles and polyaniline nanorods for nitrogen photofixation. *New J. Chem.* **2020**, *44*, 7350–7356. [[CrossRef](#)]
127. Zhang, H.; Liu, Q.; Chen, Y.; Pei, L.; Bao, L.; Yuan, Y.-J. Mixed-Valent Cobalt-Modulated Tungsten Trioxide Nanorod Arrays for Improved Photocatalytic N₂ Fixation. *J. Phys. Chem. C* **2021**, *125*, 21997–22005. [[CrossRef](#)]
128. Ying, Z.; Chen, S.; Zhang, S.; Peng, T.; Li, R. Efficiently enhanced N₂ photofixation performance of sea-urchin-like W₁₈O₄₉ microspheres with Mn-doping. *Appl. Catal. B* **2019**, *254*, 351–359. [[CrossRef](#)]
129. Wang, T.; Qu, S.; Wang, J.; Xu, M.; Qu, C.; Feng, M. W/Mo-heteropoly blue-modified defective W₁₈O₄₉ as Z-Scheme heterostructure photocatalysts for efficient N₂ fixation. *J. Alloys Compd.* **2023**, *938*, 168631. [[CrossRef](#)]
130. Wang, L.; Wang, S.; Cui, D.; Li, M.; Yang, X.; Li, F.; Xu, L. Z-scheme heterojunctions with double vacancies semiconductors MoO_{3-x} and Fe-doped W₁₈O₄₉ for photocatalytic nitrogen fixation. *J. Alloys Compd.* **2022**, *927*, 167003. [[CrossRef](#)]
131. Sun, B.; Qiu, P.; Liang, Z.; Xue, Y.; Zhang, X.; Yang, L.; Cui, H.; Tian, J. The fabrication of 1D/2D CdS nanorod@Ti₃C₂ MXene composites for good photocatalytic activity of hydrogen generation and ammonia synthesis. *Chem. Eng. J.* **2021**, *406*, 127177. [[CrossRef](#)]
132. Sun, B.; Liang, Z.; Qian, Y.; Xu, X.; Han, Y.; Tian, J. Sulfur Vacancy-Rich O-Doped 1T-MoS₂ Nanosheets for Exceptional Photocatalytic Nitrogen Fixation over CdS. *ACS Appl. Mater. Interfaces* **2020**, *12*, 7257–7269. [[CrossRef](#)] [[PubMed](#)]

Disclaimer/Publisher’s Note: The statements, opinions and data contained in all publications are solely those of the individual author(s) and contributor(s) and not of MDPI and/or the editor(s). MDPI and/or the editor(s) disclaim responsibility for any injury to people or property resulting from any ideas, methods, instructions or products referred to in the content.